cells or precursor cells, DNA methylation alterations are stably preserved on DNA double strands by covalent bonds. Therefore, even subtle alterations at the precancerous stage can be detected using highly sensitive methodology. DNA methylation alterations may be optimal indicators for carcinogenetic risk estimation.[12,13]

We have already established criteria for estimation of the risk of HCC development using bacterial artificial chromosome (BAC) array-based methylated CpG island amplification (BAMCA),[14–19] which can provide an overview of the DNA methylation tendency of individual large regions among all chromosomes;[13,19] 25 BAC clones, whose DNA methylation status was able to discriminate noncancerous liver tissue obtained from patients with HCCs in the learning cohort from normal liver tissue obtained from patients without HCCs, were identified.[18] However, sensitivity and specificity of such discrimination were not 100% in the validation cohort. Moreover, the CpG sites that are of diagnostic importance are unclear on each of the BAC clones with an average insert size of 170 kbp.[20] As the technique of BAMCA requires a large amount of genomic DNA and is somewhat cumbersome, risk estimation using BAMCA may be difficult to apply in a clinical setting.

Here, to identify precisely the CpG sites having the largest diagnostic impact, we quantitatively evaluated the DNA methylation status of 203 CpG sites on these 25 BAC clones using pyrosequencing in tissue specimens. Among the CpG sites, we were able to improve the specificity of carcinogenetic risk estimation by combining those showing the largest diagnostic impact and to apply such risk estimation to a very small amount of genomic DNA with a view to clinical application.

Material and Methods

Patients and tissue samples

As a learning cohort, 10 samples of normal liver tissue (C1–C10) showing no remarkable histological findings were obtained from specimens surgically resected from 10 patients without HCCs who were negative for both HBV surface antigen (HBs-Ag) and anti-HCV antibody (anti-HCV). The patients comprised seven men and three women with a mean (± standard deviation) age of 58.4 ± 9.7 years. Nine patients underwent partial hepatectomy for liver metastases of primary colon cancer, and one patient did so for liver metastases of a gastrointestinal stromal tumor of the stomach at the National Cancer Center Hospital, Tokyo, Japan. A total of 12 samples of noncancerous liver tissue (N1–N12) were obtained from 12 patients who underwent partial hepatectomy for HCCs. These patients comprised nine men and three women with a mean age of 65.3 ± 6.4 years. Among them, six were positive for HBs-Ag and six were positive for anti-HCV. Histological examination of these noncancerous liver tissue samples revealed findings compatible with chronic hepatitis in four and cirrhosis in eight.

As a validation cohort, 45 samples of normal liver tissue (C11–C55) exhibiting no remarkable histological findings were obtained from 45 patients without HCCs who were negative for both HBs-Ag and anti-HCV. The patients comprised 34 men and 11 women with a mean age of 62.2 ± 7.0 years. A total of 39 patients underwent partial hepatectomy for liver metastases from primary colon cancer, three patients did so for liver metastasis from gastric cancer and the remaining three patients did so for liver metastasis from each of gastrointestinal stromal tumor of the stomach, pancreatic cancer and colon carcinoid tumor, respectively. A total of 45 samples of noncancerous liver tissue (N13–N57) were obtained from 45 patients who underwent partial hepatectomy for HCCs. The patients comprised 37 men and eight women with a mean age of 62.3 ± 9.7 years. Of them 13 were positive for HBs-Ag, 29 were positive for anti-HCV, and three were negative for both. Histological examination of these noncancerous liver tissue samples revealed findings compatible with chronic hepatitis in 22 and cirrhosis in 23.

For comparison, 34 samples of primary HCC (T1–T34) were also obtained from specimens surgically resected from the patients who had provided the samples N1–N34. In addition, for comparison, 14 samples of liver tissue (V1–V14) were obtained from 14 patients who were positive for HBs-Ag or anti-HCV, but who had never developed HCCs. The patients comprised six men and eight women with a mean age of 65.1 ± 8.2 years. Of them, 12 patients underwent partial hepatectomy for liver metastases of primary colorectal cancer and two patients did so for liver metastases of gastric cancer.

Our study was approved by the Ethics Committee of the National Cancer Center, Tokyo, Japan. All the patients gave informed consent before their inclusion in our study.

DNA extraction and bisulfite DNA modification

High-molecular-weight DNA from fresh-frozen tissue samples was extracted using phenol–chloroform followed by dialysis. Bisulfite conversion was carried out using 1 μg of genomic DNA and the reagents provided in the EpiTect Bisulfite Kit (QIAGEN GmbH, Hilden, Germany), in accordance with the manufacturer's protocol. This process converts unmethylated cytosine residues to uracil, whereas methylated cytosine residues remain unchanged.[21]

Pyrosequencing DNA methylation analysis

DNA methylation level was measured by a highly quantitative method using Pyrosequencing™ technology. Polymerase chain reaction (PCR) and sequencing primers were designed based on the converted sequences using Pyrosequencing Assay Design Software ver.1.0 (QIAGEN GmbH). To overcome PCR bias in DNA methylation analysis, we optimized the annealing temperature as described previously.[22,23] Each of the primer sequences and PCR conditions are given in Supporting Information Table 1. The PCR was carried out with 0.6 units of AmpliTaq Gold (Applied Biosystems, Foster City, CA) using 7.5 ng of bisulfite-treated DNA. The

Table 1. Thirty regions that were able to discriminate noncancerous liver tissues (N) from normal liver tissues (C)

Region	BAC clone ID	Location	Characteristics	Gene	Cutoff value (%)	DNA methylation status[1]	Sensitivity (%)	Specificity (%)
1	RP11–104J13	1p35.2	Noncoding/CpG island	None	25.5	C > N	80.0	66.7
2	RP11–104J13	1p35.2	Noncoding	None	26.0	C > N	90.0	91.7
3	RP11–104J13	1p35.2	First intron/CpG island	SDC3	34.0	C > N	90.0	91.7
4	RP11–104J13	1p35.2	Noncoding	None	88.9	C < N	100	66.7
5	RP11–52I2	1p33	First exon/CpG island	FOXD2	47.5	C > N	90.0	91.7
6	RP11–29M22	1p12	Intron	PHGDH	73.0	C < N	100	50.0
7	RP11–21K1	2q37.1	Noncoding	None	93.0	C > N	80.0	50.0
8	RP11–109B15	5q33.1	Noncoding	None	12.0	C < N	80.0	83.3
9	RP11–112B7	7p13	First intron/CpG island	CAMK2B	45.0	C > N	20.0	91.7
10	RP11–120E20	11p15.4	Intron	ART5	85.0	C > N	50.0	100
11	RP11–120E20	11p15.4	Intron/SINE repeat	NUP98	95.7	C < N	100	75.0
12	RP11–334E6	11q23.3	First exon/CpG island	C1QTNF5	23.7	C < N	100	25.0
13	RP11–334E6	11q23.3	First intron/CpG island	THY1	12.6	C > N	60.0	83.3
14	RP11–17M17	11q25	First intron	OPCML	74.0	C > N	100	91.7
15	RP11–17M17	11q25	First intron	OPCML	79.0	C > N	100	33.3
16	RP11–17M17	11q25	First intron	OPCML	49.7	C > N	70.0	50.0
17	RP11–319E16	12p13.32	Noncoding	None	79.0	C > N	70.0	58.3
18	RP11–319E16	12p13.32	Noncoding/SINE repeat	None	45.0	C > N	100	50.0
19	RP11–1100L3	12q13.13	UTR	ACVRL1	50.0	C < N	90.0	83.3
20	RP11–1100L3	12q13.13	Promoter/CpG island	GRASP	7.0	C > N	80.0	58.3
21	RP11–799O6	12q13.3	UTR	ZBTB39	40.0	C < N	100	91.7
22	RP11–799O6	12q13.3	Noncoding/SINE repeat	None	89.0	C < N	80.0	100
23	RP11–89M4	16p13.3	Noncoding	None	38.0	C < N	70.0	100
24	RP11–89M4	16p13.3	Intron	LOC342346	69.0	C > N	100	33.3
25	RP11–89M4	16p13.3	Exon/CpG island	MGRN1	51.0	C < N	100	100
26	RP11–89M4	16p13.3	Intron	MGRN1	28.0	C < N	100	50.0
27	RP11–89M4	16p13.3	Intron/CpG island	MGRN1	67.0	C < N	100	100
28	RP11–348B12	19p13.3	Intron/CpG island	KDM4B	44.0	C < N	100	100
29	RP11–348B12	19p13.3	Intron/CpG island	KDM4B	94.8	C < N	100	41.7
30	RP11–348B12	19p13.3	Intron/CpG island	KDM4B	94.0	C > N	50.0	91.7

[1]C > N, when the signal ratio was lower than the cutoff value, the tissue sample was considered to be at high risk for carcinogenesis; C < N, when the signal ratio was higher than the cutoff value, the tissue sample was considered to be at high risk for carcinogenesis.

biotinylated PCR product was captured on streptavidin-coated beads (Streptavidin Sepharose™ High Performance; GE Healthcare, Uppsala, Sweden). Quantitative sequencing was run on the PyroMark Q24 (QIAGEN GmbH) using the Pyro Gold Reagents (QIAGEN GmbH) in accordance with the manufacturer's protocol. For each assay, the setup included positive controls (Epitect methylated human control DNA; QIAGEN GmbH) and negative controls (Epitect unmethylated human control DNA; QIAGEN GmbH). The PCR products were separated electrophoretically on 3% agarose gel and stained with ethidium bromide to confirm that specific products of the appropriate size and no nonspecific products were obtained on amplification. Representative pyrograms are shown in Figure 1.

As outlined in Figure 1, the DNA methylation level (%) at each CpG site is given by the following formula:

$$\text{luminescence strength of cytosine} / (\text{luminescence strength of cytosine} + \text{luminescence strength of thymine}) \times 100.$$

Statistics

Significant differences in DNA methylation levels at each of the CpG sites between groups of samples were analyzed using the Mann-Whitney *U* test. Survival curves of patient groups with HCCs were calculated by the Kaplan–Meier method,

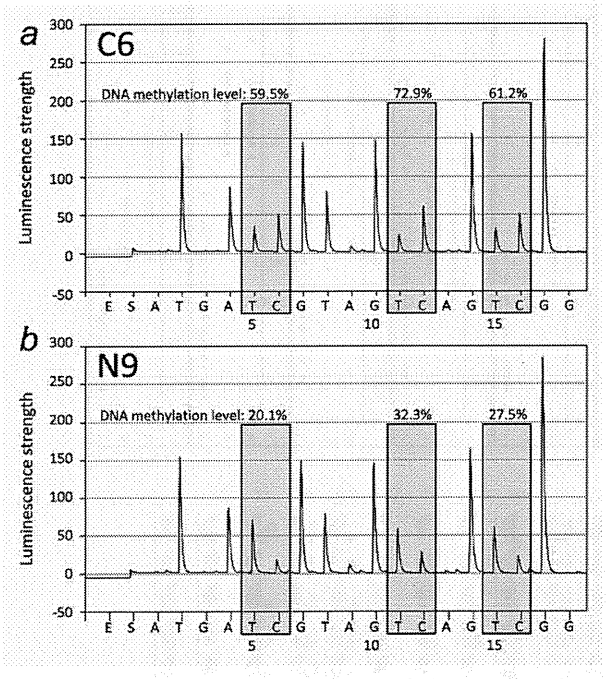

Figure 1. Pyrosequencing DNA methylation analysis. Examples of pyrograms for a sample of normal liver tissue obtained from a patient without HCC (C6) and a sample of noncancerous liver tissue obtained from a patient with HCC (N9) for exon 1 of the *FOXD2* gene (47,677,654, −60, −63 in region 5 in Table 1). Gray columns represent the regions of polymorphic sites after bisulfite modification. *x*-axis indicates dispensation order (time).

and the differences were compared by log-rank test. Differences at $p < 0.05$ were considered significant.

Results

Validation of BAMCA data by pyrosequencing

It has been shown that BAMCA can provide an overview of the DNA methylation tendency of individual large regions among all chromosomes.[13,19] Therefore, using pyrosequencing, we evaluated the DNA methylation levels of all *Xma* I/*Sma* I sites, which yielded less than 2,000 bp PCR products that are effective in BAMCA, on representative BAC clones, which had been identified as indicators for carcinogenetic risk estimation in our previous study.[18] For example, on clone RP11-17M17, there were 10 *Xma* I/*Sma* I sites that were effective in BAMCA (Fig. 2*a*). The average signal ratio by BAMCA of this BAC clone was significantly lower in samples of noncancerous liver tissue obtained from patients with HCCs than in samples of normal liver tissue and was significantly lower in HCCs than in samples of noncancerous liver tissue obtained from patients with HCCs in our previous study.[18] The average DNA methylation levels determined by pyrosequencing of all 10 *Xma* I/*Sma* I sites on this BAC clone in 34 samples of noncancerous liver tissue obtained from patients with HCCs were the same as (*Xma* I/*Sma* I sites i, ii, vii, viii and ix in Fig. 2*a*) or significantly lower than (iii, iv, v, vi and x in Fig. 2*a*) those in 35 samples of normal liver tissue. Moreover, the DNA methylation levels of all *Xma* I/*Sma* I sites in 34 HCCs were significantly lower than those in samples of noncancerous liver tissue obtained from patients with HCCs (i–x in Fig. 2*a*). DNA methylation levels of CpG sites adjacent to the *Xma* I/*Sma* I sites that were quantitatively sequenced using the same sequencing primers tended to be close to the DNA methylation levels of the *Xma* I/*Sma* I sites themselves in each sample, such as iii and iii′ and iv and iv′ in Figure 2*b*. Thus, it was confirmed that BAMCA was able to successfully reveal DNA methylation alterations occurring in a coordinated manner on RP11-17M17. In another BAC clone, RP11-799O6, which was also identified as an indicator for carcinogenetic risk estimation, the average signal ratio obtained by BAMCA was significantly higher in samples of noncancerous liver tissue from patients with HCCs than in samples of normal liver tissue in our previous study.[18] Although the average DNA methylation levels of seven out of 10 *Xma* I/*Sma* I sites, which yielded PCR products of less than 2,000 bp that are effective for BAMCA, by pyrosequencing in samples of noncancerous liver tissue from patients with HCCs were the same as those in samples of normal liver tissue, those of the remaining three *Xma* I/*Sma* I sites in samples of noncancerous liver tissue obtained from patients with HCCs were markedly higher than those in samples of normal liver tissue (data not shown). Thus, pyrosequencing data again validated the BAMCA data for BAC clones identified as indicators for carcinogenetic risk estimation.

Criteria for carcinogenetic risk estimation using liver tissue samples based on pyrosequencing

To identify CpG sites having the largest diagnostic impact, DNA methylation levels of 203 CpG sites were measured by pyrosequencing using primer sets encompassing *Xma* I/*Sma* I sites, which were effective in BAMCA, on the 25 BAC clones on which we based our previous criteria.[18]

On 59 CpG sites, the average DNA methylation levels differed significantly between normal liver tissue and noncancerous liver tissue obtained from patients with HCCs in the learning cohort using Mann-Whitney *U* test ($p < 0.001$). To establish reproducible criteria, 14 CpG sites whose average DNA methylation levels in both normal liver tissue and noncancerous liver tissue obtained from patients with HCCs were less than 10% were omitted from the list of candidate indicators for carcinogenetic risk estimation, taking the characteristics of Pyrosequencing™ technology into consideration.[22] Figure 3*a* shows scattergrams of the DNA methylation levels in samples of normal liver tissue and noncancerous liver tissue obtained from patients with HCCs on representative CpG sites. Using the cutoff values described in each panel, noncancerous liver tissue obtained from patients with

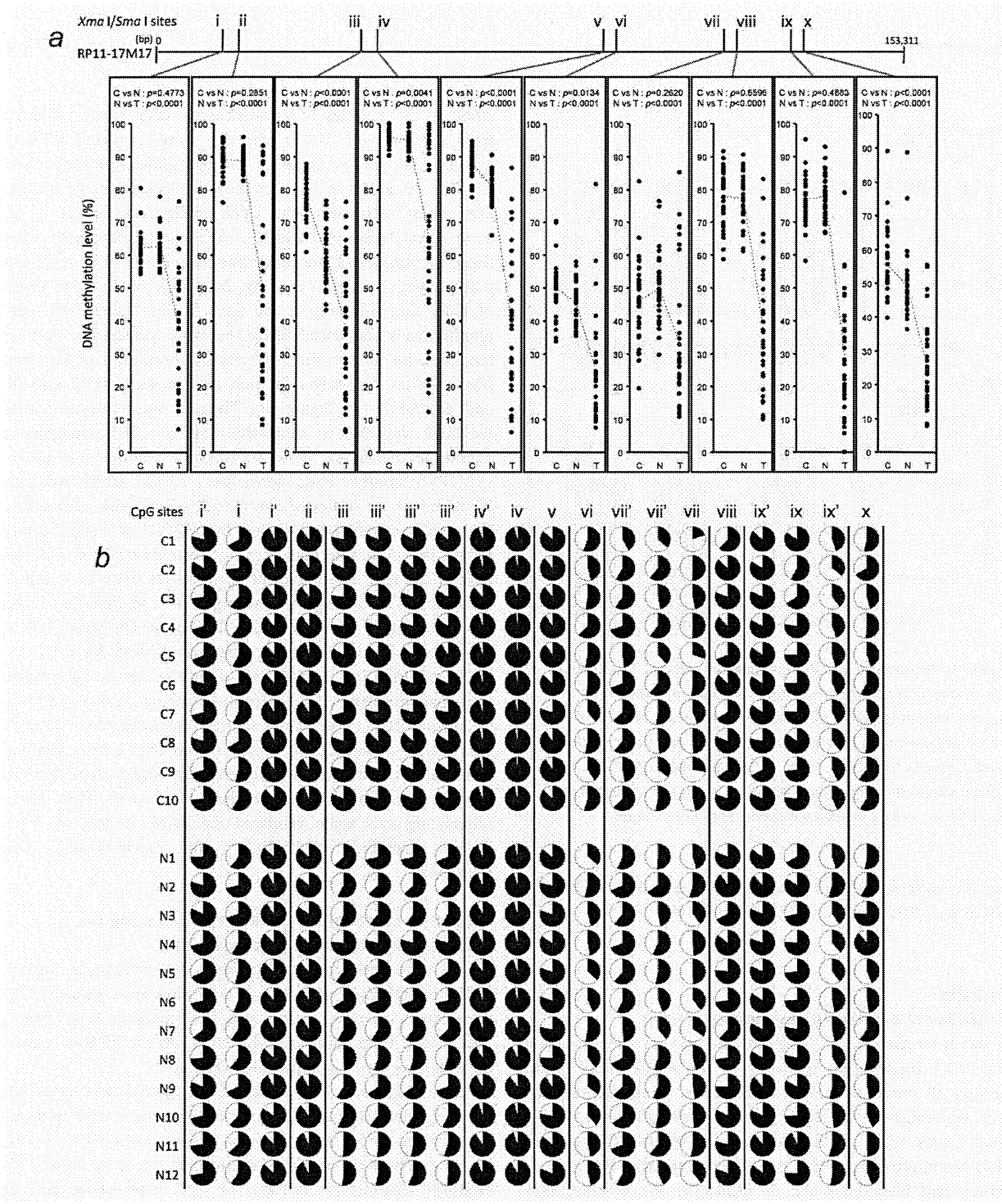

Figure 2. Validation of BAMCA data by pyrosequencing. On RP11-17M17 clone, there were 10 *Xma* I/*Sma* I sites (i–x) that yielded PCR products of less than 2,000 bp that were effective in BAMCA. The average signal ratio obtained by BAMCA for this BAC clone was significantly lower in samples of noncancerous liver tissue obtained from patients with HCCs (N) than in those of normal liver tissue (C) and was significantly lower in HCCs than in N-samples.[18] (*a*) Scattergrams of DNA methylation levels analyzed by pyrosequencing in C-samples (C1–C35), N-samples (N1–N34) and HCCs (T1–T34) on each *Xma* I/*Sma* I site. The average DNA methylation levels obtained by pyrosequencing for all 10 *Xma* I/*Sma* I sites on this BAC clone in 34 N-samples were the same as (on i, ii, vii, viii and ix) or significantly lower than (on iii, iv, v, vi and x) those in 35 C-samples. Moreover, DNA methylation levels in 34 HCCs were significantly lower than those in N-samples (on i–x). (*b*) Pi-charts of DNA methylation levels in C-samples (C1–C10) and N-samples (N1–N12) for each of the CpG sites. CpG sites adjacent to the *Xma* I/*Sma* I site (i, iii, iv, vii and ix), which were quantitatively sequenced using the same sequencing primers, are indicated by i′, iii′, iv′, vii′ and ix′, respectively. White indicates unmethylated cytosine and black indicates methylated cytosine. DNA methylation levels of CpG sites adjacent to the *Xma* I/*Sma* I sites tend to be close to the DNA methylation levels of the *Xma* I/*Sma* I sites themselves, *e.g.*, iii and iii′ and iv and iv′, in each sample.

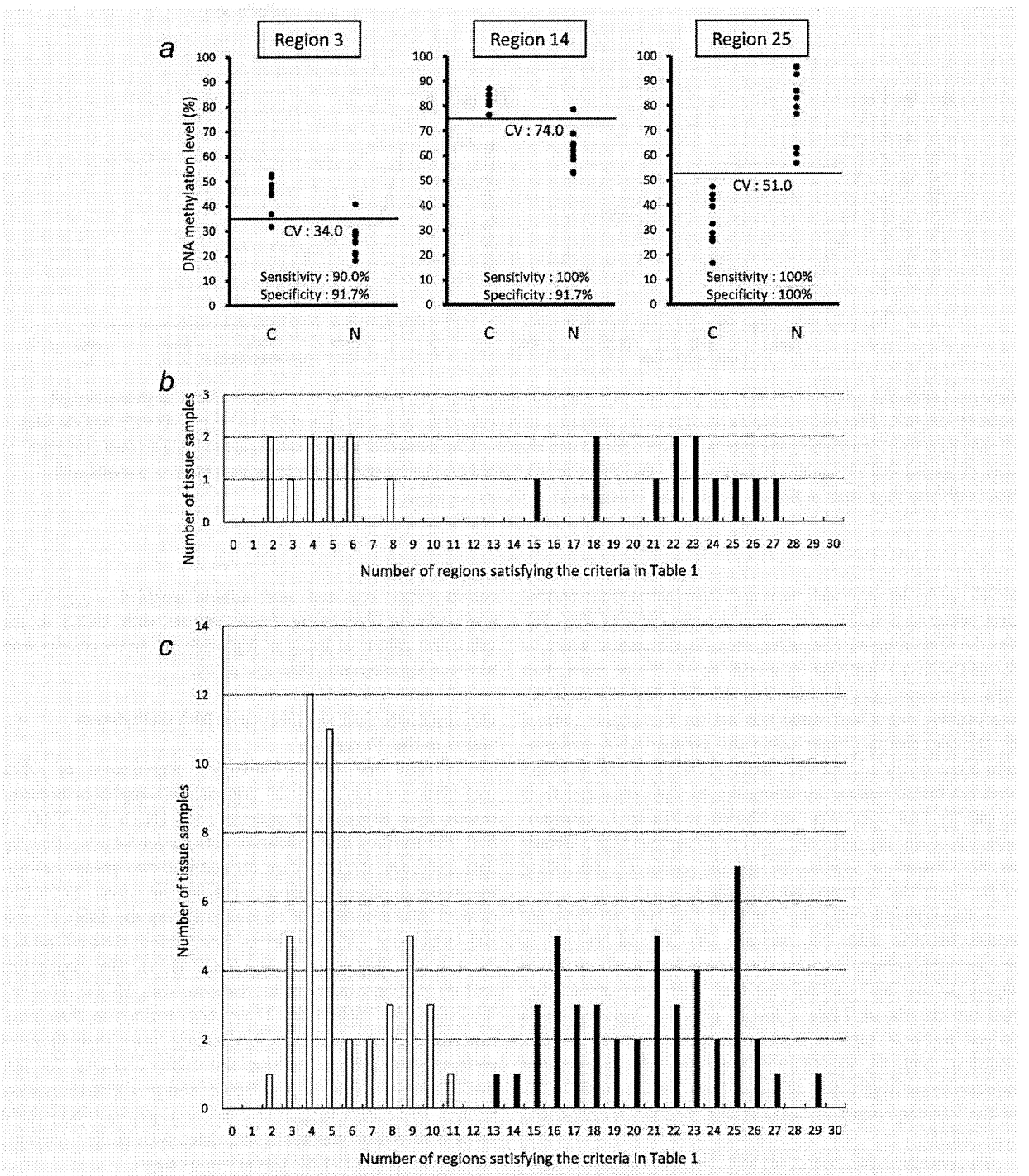

Figure 3. The criteria for carcinogenetic risk estimation based on pyrosequencing. (*a*) Scattergrams of DNA methylation levels in samples of normal liver tissue (C1–C10) and samples of noncancerous liver tissue obtained from patients with HCCs (N1–N12) in the learning cohort for representative regions. Using the cutoff values (CV, %) described in each panel, N-samples in the learning cohort were discriminated from C-samples with sufficient sensitivity and specificity. (*b*) Histogram showing the number of regions satisfying the criteria described in Table 1 in samples C1–C10 (clear columns) and N1–N12 (filled columns). On the basis of this histogram, we judged that when the noncancerous liver tissue satisfied the criteria in Table 1 for 15 or more than 15 regions, it was at high risk of carcinogenesis. (*c*) Validation of the criteria in Table 1 using an additional 90 samples of liver tissue in the validation cohort. All 43 validation samples satisfying the Table 1 criteria for 15 or more regions were N-samples (N13–N36, N38–N41 and N43–N57, filled columns), and 45 of 47 validation samples satisfying the Table 1 criteria for less than 15 regions were C-samples (C11–C55, clear columns). DNA methylation statuses for the 30 regions of N-samples and those of C-samples were completely mutually exclusive in the validation cohort.

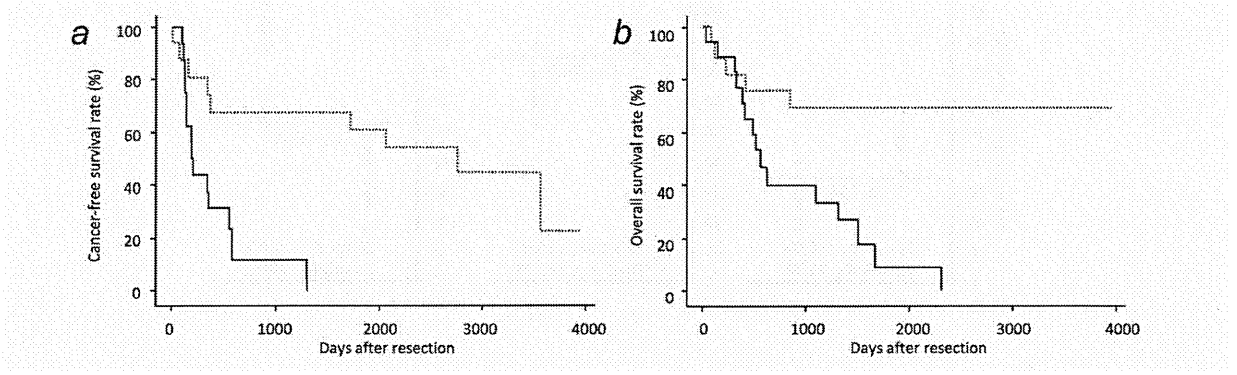

Figure 4. Correlation between DNA methylation status at the precancerous stage and patient outcome. Kaplan–Meier survival curves of patients with HCCs from whom samples N1–N34 were obtained. The cancer-free (*a*; $p = 0.0023$) and overall (*b*; $p = 0.0015$) survival rates of patients with HCCs satisfying the criteria in Table 1 for 23 (the median of the number of regions satisfying the Table 1 criteria) or more than 23 regions in their samples of noncancerous liver tissue ($n = 17$, solid lines) were significantly lower than those of patients with HCCs satisfying the criteria in Table 1 for less than 23 regions ($n = 17$, broken lines).

HCCs in the learning cohort was discriminated from normal liver tissue with sufficient sensitivity and specificity (Fig. 3*a*). On the remaining 45 CpG sites, such discrimination was performed with a sensitivity or specificity of 70% or more than 70%. If several CpG sites were measured using one sequencing primer, one cutoff value was set for the region covered by the sequencing primer using the average DNA methylation levels of the several CpG sites. Then the 30 cutoff values were set for 30 regions including the 45 CpG sites, and their sensitivity and specificity are shown in Table 1. Chromosomal loci and characteristics of the 30 regions (CpG islands or not, exons or introns of specific genes or noncoding regions) are also summarized in Table 1.

A histogram showing the number of regions satisfying the criteria listed in Table 1 for samples C1–C10 and N1–N12 in the learning cohort is shown in Figure 3*b*. On the basis of Figure 3*b*, we finally established that when liver tissue satisfied the criteria in Table 1 for 15 or more regions, it was judged to be at high risk of carcinogenesis. Based on this definition both the sensitivity and specificity for diagnosis of noncancerous liver tissue obtained from patients with HCCs in the learning cohort as being at high risk of carcinogenesis were 100%.

To confirm these criteria, an additional 90 samples of liver tissue were analyzed by pyrosequencing as a validation study (Fig. 3*c*). All of the 43 validation samples satisfying the criteria in Table 1 for 15 or more regions were noncancerous liver tissue obtained from patients with HCCs (N13–N36, N38–N41 and N43–N57), and 45 of the 47 validation samples satisfying the Table 1 criteria for less than 15 regions were normal liver tissue (C11–C55). DNA methylation statuses for the 30 regions of noncancerous liver tissue samples from patients with HCCs and those of normal liver tissue samples were completely mutually exclusive in the validation cohort (Fig. 3*c*), and our criteria enabled diagnosis of noncancerous liver tissue from patients with HCCs in the validation cohort as being at high risk of carcinogenesis with 95.6% sensitivity and 100% specificity.

Clinicopathological significance of DNA methylation status in the 30 regions

To estimate the clinicopathological significance of DNA methylation status in the 30 regions, 34 samples of noncancerous liver tissue from patients with HCCs (N1–N34) in both the learning and validation cohorts for whom follow-up data had been obtained were divided into two groups according to the number of regions satisfying the criteria (≥23 [the median of the number of regions satisfying the Table 1 criteria] regions *vs.* <23 regions). The period covered ranged from 11 to 3,936 days (mean: 1,417 days). The cancer-free and overall survival rates for patients with HCCs satisfying the criteria in Table 1 for 23 or more regions in their noncancerous liver tissue were significantly lower than those of patients with HCCs satisfying the Table 1 criteria for less than 23 regions (Fig. 4, $p = 0.0023$ and $p = 0.0015$, respectively). These data suggested that clinicopathologically valid DNA methylation alterations associated with patient outcome are already present at the precancerous stage.

With respect to all 57 samples of noncancerous liver tissue (N1–N57), the difference in the number of regions satisfying the criteria listed in Table 1 between liver tissue samples showing chronic hepatitis ($n = 26$, 19.6 ± 3.7) and those showing cirrhosis ($n = 31$, 22.0 ± 3.9) was marginal ($p = 0.0206$). For comparison, the DNA methylation levels of 30 regions in 14 additional liver tissue samples (V1–V14) obtained from patients who were infected with HBV or HCV, but who had never developed HCCs, were analyzed by pyrosequencing. The average number of regions satisfying the

Table 1 criteria was significantly lower in V1–V14 (12.0 ± 5.0), than in N1–N57 (20.9 ± 4.0, $p < 0.0001$). These data suggested that our criteria do not simply reflect the presence of hepatitis virus infection, inflammation or fibrosis at the chronic hepatitis and liver cirrhosis stages, but in fact reflect the carcinogenetic risk itself.

Discussion

For appropriate surveillance of patients at the precancerous stage for HCCs, the criteria for carcinogenetic risk estimation should be explored. As considerable numbers of liver tissue samples obtained from patients with HBV or HCV infection indicate a future risk of HCCs, even if HCCs are not yet present, comparison between liver tissue samples obtained from patients with HBV or HCV infection but without HCCs and those obtained from patients with HBV or HCV infection but also showing HCCs, is not an adequate strategy for establishing criteria for carcinogenetic risk estimation. Therefore, in our previous study, we focused on BAC clones whose signal ratios differed significantly between samples of normal liver tissue obtained from patients without HBV or HCV infection and samples of noncancerous liver tissue obtained from patients with HCCs (namely BAC clones on which DNA methylation alterations had occurred at the precancerous stage), and also those on which such DNA methylation alterations had been inherited by HCCs themselves from precancerous conditions. In this way, we successfully established such criteria using BAC array-based methods.[18]

In our study, the reliability of BAMCA was again confirmed: BAMCA was able to provide an overview of DNA methylation tendency in large regions of chromosomes, and especially was able to detect DNA methylation alterations occurring in a coordinated manner in the entire BAC region. However, the exact CpG sites that are of diagnostic impact are unclear, because several *Xma* I/*Sma* I sites that are effective in BAMCA generally exist on each of the BAC clones with an average insert size of 170 kbp.[20] Moreover, as BAMCA requires a large amount of genomic DNA, and the technique is somewhat cumbersome, our previous criteria based on BAMCA may not be suitable for clinical uses such as risk estimation based on liver biopsy specimens. Therefore, we employed Pyrosequencing™ technology, which is an excellent tool for quantitative estimation of DNA methylation levels at specific CpG sites.

Although numerous *Xma* I/*Sma* I sites are located within CpG islands, one or two *Xma* I/*Sma* I sites on each CpG island were analyzed because of difficulties with the design of the PCR and sequencing primers. Then, DNA methylation levels at 203 CpG sites on the 25 BAC clones that comprised our previous criteria based on BAMCA were evaluated quantitatively by pyrosequencing. By combining the 30 regions including 45 specific CpG sites, which were revealed to have a large diagnostic impact, the specificity of the criteria for carcinogenetic risk estimation was successfully improved in comparison with our previous criteria based on BAMCA[18]: the sensitivity and specificity of the criteria after revision by pyrosequencing were both 100% in the learning cohort and were 95.6% and 100% in the validation cohort, respectively.

Only one region (region 20 in Table 1) among 30 regions that had been used for defining the revised criteria for carcinogenetic risk estimation was located within the promoter region of a specific gene (general receptor for phosphoinositides 1-associated scaffold protein), although DNA methylation alterations in promoter regions are known to be one of most consistent epigenetic changes in human cancers.[24] At the risk stage, but not in established cancers, it is feasible that DNA methylation alterations do not expand immediately to the promoter regions of specific genes, such as tumor-related genes. However, 20, 19 and 9 regions that had been used for defining the revised criteria were located within gene bodies, non-CpG islands, and noncoding regions, respectively, which have been overlooked as targets of DNA methylation alterations during multistage human carcinogenesis. Although most of the recently developed detection technologies, such as promoter arrays and CpG island arrays, are sequence-based methods and cannot comprehensively measure the DNA methylation status of gene bodies, non-CpG islands and noncoding regions,[25,26] our findings indicate that meticulous examination of such sequences is also important for establishment of optimal diagnostic indicators.

DNA methylation status in the 30 regions in noncancerous liver tissue at the precancerous stage was significantly correlated with both cancer-free and overall survival rates of patients with HCCs (Fig. 4). Although prognostication before development of HCCs was not a clinically relevant issue, and we never intended to perform such prognostication, we can consider that DNA methylation alterations determining patient outcome had already accumulated at the precancerous stage, based on the data in Figure 4. As DNA methylation status is not randomly altered at the precancerous stage, and DNA methylation profiles in noncancerous liver tissue have been proven to be clinicopathologically valid, it is feasible that such profiles could be optimal indicators for carcinogenetic risk estimation.

The difference in the number of regions satisfying the criteria listed in Table 1 between liver tissue samples showing chronic hepatitis and those showing cirrhosis was marginal, indicating that our criteria were not simply associated with inflammation or fibrosis. In addition, the average number of regions satisfying the Table 1 criteria were significantly lower in liver tissue from patients without HCCs (V1–V14) than in noncancerous liver tissue from patients with HCCs (N1–N34), even though the patients from whom V1–V14 were obtained were infected with HBV or HCV. DNA methylation status in the 30 regions does not depend on hepatitis virus infection but may actually reflect the carcinogenetic risk itself. Therefore, our criteria not only discriminate noncancerous liver tissue from patients with HCCs from normal liver tissues but also may be applicable for classifying liver tissue obtained from patients who are being followed up

because of HBV or HCV infections, chronic hepatitis or cirrhosis into that which may generate HCCs and that which will not.

During surveillance at the precancerous stage, to reveal the baseline liver histology, microscopic examination of liver biopsy specimens is performed in patients with HBV or HCV infection before interferon therapy.[27,28] Therefore, carcinogenetic risk estimation using such liver biopsy specimens will be advantageous for close follow-up of patients who are at high risk of HCC development. We have confirmed that pyrosequencing can be performed using a very small amount of degraded DNA extracted from formalin-fixed and paraffin-embedded liver biopsy specimens (unpublished data). We now intend to prospectively validate the reliability of risk estimation based on the revised criteria using pyrosequencing in liver biopsy specimens obtained before interferon therapy from a large cohort of patients with HBV or HCV infection.

Acknowledgements

Author R.N. received a Research Resident Fellowship from the Foundation for Promotion of Cancer Research in Japan.

References

1. Chang MH, Chen CJ, Lai MS, Hsu HM, Wu TC, Kong MS, Liang DC, Shau WY, Chen DS. Universal hepatitis B vaccination in Taiwan and the incidence of hepatocellular carcinoma in children. Taiwan Childhood Hepatoma Study Group. *N Engl J Med* 1997;336:1855–9.
2. Tanaka Y, Hanada K, Mizokami M, Yeo AE, Shih JW, Gojobori T, Alter HJ. Inaugural article: a comparison of the molecular clock of hepatitis C virus in the United States and Japan predicts that hepatocellular carcinoma incidence in the United States will increase over the next two decades. *Proc Natl Acad Sci USA* 2002; 99:15584–9.
3. Jones PA, Baylin SB. The epigenomics of cancer. *Cell* 2007;128:683–92.
4. Sharma S, Kelly TK, Jones PA. Epigenetics in Cancer. *Carcinogenesis* 2009;31:27–36.
5. Kanai Y, Hirohashi S. Alterations of DNA methylation associated with abnormalities of DNA methyltransferases in human cancers during transition from a precancerous to a malignant state. *Carcinogenesis* 2007;28:2434–42.
6. Kanai Y. Alterations of DNA methylation and clinicopathological diversity of human cancers. *Pathol Int* 2008;58:544–58.
7. Kanai Y, Ushijima S, Tsuda H, Sakamoto M, Sugimura T, Hirohashi S. Aberrant DNA methylation on chromosome 16 is an early event in hepatocarcinogenesis. *Jpn J Cancer Res* 1996;87:1210–7.
8. Kondo Y, Kanai Y, Sakamoto M, Mizokami M, Ueda R, Hirohashi S. Genetic instability and aberrant DNA methylation in chronic hepatitis and cirrhosis—a comprehensive study of loss of heterozygosity and microsatellite instability at 39 loci and DNA hypermethylation on 8 CpG islands in microdissected specimens from patients with hepatocellular carcinoma. *Hepatology* 2000;32:970–9.
9. Kaneto H, Sasaki S, Yamamoto H, Itoh F, Toyota M, Suzuki H, Ozeki I, Iwata N, Ohmura T, Satoh T, Karino Y, Satoh T, et al. Detection of hypermethylation of the p16(INK4A) gene promoter in chronic hepatitis and cirrhosis associated with hepatitis B or C virus. *Gut* 2001; 48:372–7.
10. Saito Y, Kanai Y, Sakamoto M, Saito H, Ishii H, Hirohashi S. Overexpression of a splice variant of DNA methyltransferase 3b, DNMT3b4, associated with DNA hypomethylation on pericentromeric satellite regions during human hepatocarcinogenesis. *Proc Natl Acad Sci USA* 2002;99:10060–5.
11. Saito Y, Kanai Y, Nakagawa T, Sakamoto M, Saito H, Ishii H, Hirohashi S. Increased protein expression of DNA methyltransferase (DNMT) 1 is significantly correlated with the malignant potential and poor prognosis of human hepatocellular carcinomas. *Int J Cancer* 2003;105:527–32.
12. Kanai Y. Genome-wide DNA methylation profiles in precancerous conditions and cancers. *Cancer Sci* 2009;101:36–45.
13. Arai E, Kanai Y. DNA methylation profiles in precancerous tissue and cancers: carcinogenetic risk estimation and prognostication based on DNA methylation status. *Epigenomics* 2010;2: 467–81.
14. Misawa A, Inoue J, Sugino Y, Hosoi H, Sugimoto T, Hosoda F, Ohki M, Imoto I, Inazawa J. Methylation-associated silencing of the nuclear receptor 1I2 gene in advanced-type neuroblastomas, identified by bacterial artificial chromosome array-based methylated CpG island amplification. *Cancer Res* 2005;65:10233–42.
15. Sugino Y, Misawa A, Inoue J, Kitagawa M, Hosoi H, Sugimoto T, Imoto I, Inazawa J. Epigenetic silencing of prostaglandin E receptor 2 (PTGER2) is associated with progression of neuroblastomas. *Oncogene* 2007;26:7401–13.
16. Tanaka K, Imoto I, Inoue J, Kozaki K, Tsuda H, Shimada Y, Aiko S, Yoshizumi Y, Iwai T, Kawano T, Inazawa J. Frequent methylation-associated silencing of a candidate tumor-suppressor, CRABP1, in esophageal squamous-cell carcinoma. *Oncogene* 2007;26:6456–68.
17. Arai E, Ushijima S, Fujimoto H, Hosoda F, Shibata T, Kondo T, Yokoi S, Imoto I, Inazawa J, Hirohashi S, Kanai Y. Genome-wide DNA methylation profiles in both precancerous conditions and clear cell renal cell carcinomas are correlated with malignant potential and patient outcome. *Carcinogenesis* 2009;30:214–21.
18. Arai E, Ushijima S, Gotoh M, Ojima H, Kosuge T, Hosoda F, Shibata T, Kondo Y, Yokoi S, Imoto I, Inazawa J, Hirohashi S, et al. Genome-wide DNA methylation profiles in liver tissue at the precancerous stage and in hepatocellular carcinoma. *Int J Cancer* 2009;125:2854–62.
19. Nishiyama N, Arai E, Chihara Y, Fujimoto H, Hosoda F, Shibata T, Kondo T, Tsukamoto T, Yokoi S, Imoto I, Inazawa J, Hirohashi S, et al. Genome-wide DNA methylation profiles in urothelial carcinomas and urothelia at the precancerous stage. *Cancer Sci* 2010;101: 231–40.
20. Osoegawa K, Mammoser AG, Wu C, Frengen E, Zeng C, Catanese JJ, de Jong PJ. A bacterial artificial chromosome library for sequencing the complete human genome. *Genome Res* 2001;11: 483–96.
21. Clark SJ, Harrison J, Paul CL, Frommer M. High sensitivity mapping of methylated cytosines. *Nucleic Acids Res* 1994;22: 2990–7.
22. Shen L, Guo Y, Chen X, Ahmed S, Issa JP. Optimizing annealing temperature overcomes bias in bisulfite PCR methylation analysis. *Bio Techniques* 2007; 42:48–58.
23. Gao W, Kondo Y, Shen L, Shimizu Y, Sano T, Yamao K, Natsume A, Goto Y, Ito M, Murakami H, Osada H, Zhang J, et al. Variable DNA methylation patterns associated with progression of disease in hepatocellular carcinomas. *Carcinogenesis* 2008;29:1901–10.
24. Baylin SB, Ohm JE. Epigenetic gene silencing in cancer—a mechanism for early oncogenic pathway addiction? *Nat Rev Cancer* 2006;6:107–16.

25. Estecio MR, Issa JP. Tackling the methylome: recent methodological advances in genome-wide methylation profiling. *Genome Med* 2009;1:106.
26. Mohn F, Schubeler D. Genetics and epigenetics: stability and plasticity during cellular differentiation. *Trends Genet* 2009; 25:129–36.
27. Arase Y, Ikeda K, Suzuki F, Suzuki Y, Kobayashi M, Akuta N, Hosaka T, Sezaki H, Yatsuji H, Kawamura Y, Kobayashi M, Kumada H. Comparison of interferon and lamivudine treatment in Japanese patients with HBeAg positive chronic hepatitis B. *J Med Virol* 2007;79: 1286–92.
28. Yoshida H, Tateishi R, Arakawa Y, Sata M, Fujiyama S, Nishiguchi S, Ishibashi H, Yamada G, Yokosuka O, Shiratori Y, Omata M. Benefit of interferon therapy in hepatocellular carcinoma prevention for individual patients with chronic hepatitis C. *Gut* 2004;53: 425–30.

Carcinogenesis vol.32 no.4 pp.462–469, 2011
doi:10.1093/carcin/bgq274
Advance Access publication December 22, 2010

Copy number alterations in urothelial carcinomas: their clinicopathological significance and correlation with DNA methylation alterations

Naotaka Nishiyama[1,2], Eri Arai[1], Ryo Nagashio[1], Hiroyuki Fujimoto[3], Fumie Hosoda[4], Tatsuhiro Shibata[4], Taiji Tsukamoto[2], Sana Yokoi[5], Issei Imoto[5], Johji Inazawa[5] and Yae Kanai[1,*]

[1]Pathology Division, National Cancer Center Research Institute, Tokyo 104-0045, Japan, [2]Division of Urology, Sapporo Medical University, Sapporo 060-8556, Japan, [3]Urology Division, National Cancer Center Hospital, Tokyo 104-0045, Japan, [4]Cancer Genomics Project, National Cancer Center Research Institute, Tokyo 104-0045, Japan and [5]Department of Molecular Cytogenetics, Medical Research Institute and School of Biomedical Science, Tokyo Medical and Dental University, Tokyo 113-8510, Japan

*To whom correspondence should be addressed. Tel: +81 3 3542 2511; Fax: +81 3 3248 2463;
Email: ykanai@ncc.go.jp

The aim of this study was to clarify the genetic backgrounds underlying the clinicopathological characteristics of urothelial carcinomas (UCs). Array comparative genomic hybridization analysis using a 244K oligonucleotide array was performed on 49 samples of UC tissue. Losses of 2q33.3–q37.3, 4p15.2–q13.1 and 5q13.3–q35.3 and gains of 7p11.2–q11.23 and 20q13.12–q13.2 were correlated with higher histological grade, and gain of 7p21.2–p21.12 was correlated with deeper invasion. Losses of 6q14.1–q27 and 17p13.3–q11.1 and gains of 19q13.12–q13.2 and 20q13.12–q13.33 were correlated with lymph vessel involvement. Loss of 16p12.2–p12.1 and gain of 3q26.32–q29 were correlated with vascular involvement. Losses of 5q14.1–q23.1, 6q14.1–q27, 8p22–p21.3, 11q13.5–q14.1 and 15q11.2–q22.2 and gains of 7p11.2–q11.22 and 19q13.12–q13.2 were correlated with the development of aggressive non-papillary UCs. Losses of 1p32.2–p31.3, 10q11.23–q21.1 and 15q21.3 were correlated with tumor recurrence. Unsupervised hierarchical clustering analysis based on copy number alterations clustered UCs into three subclasses: copy number alterations associated with genome-wide DNA hypomethylation, regional DNA hypermethylation on C-type CpG islands and genome-wide DNA hypo- and hypermethylation were accumulated in clusters A, B_1 and B_2, respectively. Tumor-related genes that may encode therapeutic targets and/or indicators useful for the diagnosis and prognostication of UCs should be explored in the above regions. Both genetic and epigenetic events appear to accumulate during urothelial carcinogenesis, reflecting the clinicopathological diversity of UCs.

Introduction

Urothelial carcinomas (UCs) are classified as superficial papillary carcinomas or non-papillary carcinomas according to their configuration (1). Papillary carcinomas usually remain non-invasive although patients need to undergo repeated urethrocystoscopic resection for recurrences. In contrast, non-papillary invasive carcinomas usually develop from widely spreading flat carcinomas *in situ* showing a higher histological grade, and their clinical outcome is poor. There is also an alternative pathway by which papillary carcinomas develop higher histological grades during repetitive recurrence and transform into non-papillary invasive carcinomas. Thus, UCs show marked clinicopathological diversity (2). In order to improve the efficiency of diagnosis and therapy, it is necessary to clarify the genetic backgrounds underlying the various clinicopathological characteristics of UCs.

Previous studies employing Southern blotting based on restriction enzyme length polymorphism, polymerase chain reaction (PCR)–loss of heterozygosity (LOH) analysis using microsatellite markers, comparative genomic hybridization (CGH) analysis and fluorescence *in situ* hybridization (FISH) have revealed chromosomal instability in UCs such as losses of 2q, 5q, 9q and 10q and gains of 5p, 7p, 8q, 11q and 20q (3–12). However, such approaches are not effective for defining the break points in detail. Although recently developed array-based technology has been applied to UCs (13–18), the resolution of the arrays employed was insufficient or correlations between copy number alterations and the clinicopathological parameters of UCs were not analyzed in detail. Therefore, the genetic backgrounds underlying urothelial carcinogenesis have not been fully clarified.

In addition, multistage carcinogenesis is known to comprise both genetic and epigenetic events (19–21). We have reported the accumulation of DNA methylation on C-type CpG islands (22) in a cancer-specific, but not age-dependent, manner and demonstrated protein overexpression of DNA methyltransferase 1, a major DNA methyltransferase, even in non-cancerous urothelia with no apparent histological changes obtained from patients with UCs (23,24), as a result of possible exposure to carcinogens in the urine at the precancerous stage. Accumulation of DNA methylation on C-type CpG islands associated with DNA methyltransferase 1 protein overexpression was more frequently evident in aggressive non-papillary UCs (23,24). DNA hypomethylation on pericentromeric satellite regions was significantly correlated with LOH on chromosome 9 in UCs (25). Moreover, we have identified optimal indicators for carcinogenetic risk estimation in histologically normal urothelia, and for prognostication in surgically resected specimens from patients with UCs (26) using the bacterial artificial chromosome array-based methylated CpG island amplification (BAMCA) method (27–29), which is suitable for overviewing the DNA methylation tendency of individual large regions among all chromosomes (30). Although these data indicated that not only genetic but also epigenetic alterations play significant roles in UC development, to our knowledge, the correlations between copy number alterations and DNA methylation profiles in UCs have not been examined in a genome-wide manner.

In the present study of 49 UCs, we analyzed copy number alterations by array CGH analysis using a high-resolution (244K) oligonucleotide array, DNA methylation alterations on a genome-wide scale using BAMCA and DNA methylation status on C-type CpG islands using bisulfite modification. We then examined the clinicopathological significance of copy number alterations and the correlations between alterations of copy number and those of DNA methylation.

Abbreviations: BAC, bacterial artificial chromosome; BAMCA, bacterial artificial chromosome array-based methylated CpG island amplification; CGH, comparative genomic hybridization; COBRA, combined bisulfite restriction enzyme analysis; FISH, fluorescence *in situ* hybridization; LOH, loss of heterozygosity; mRNA, messenger RNA; MINT, methylated in tumor; MSP, methylation-specific polymerase chain reaction; RT, reverse transcription; PCR, polymerase chain reaction; UC, urothelial carcinoma.

Material and methods

Patients and tissue samples

Forty-nine samples (T1 to T49) of UCs of the urinary bladder, ureter and renal pelvis were obtained from specimens that had been surgically resected by radical cystectomy (16 patients) or nephroureterectomy (33 patients) at the National Cancer Center Hospital, Tokyo, Japan. The patients comprised 38 men and 11 women whose mean age was 68.59 ± 10.11 (mean ± standard deviation) years (range 49–85 years). Among the UCs, 19 and 30 were graded as low- and high-grade tumors, respectively, on the basis of the World Health Organization classification (31), and 34 and 15 were classed as superficial (pTis, pTa, pT1) and invasive (pT2 or more), respectively (31). Histological examination of UCs revealed lymph vessel involvement in 16 and vascular involvement in 9. On the basis of macroscopic examination, the UCs were divided into 28 papillary tumors and 21 non-papillary tumors. Five patients were positive for lymph node metastasis at the point of radical cystectomy or nephroureterectomy. Recurrence was diagnosed by urologists mainly on the basis of computed tomography, abdominal ultrasonography and urine cytological examinations. The mean observation period was 39.7 ± 31.8 months (mean ± standard deviation) and seven patients were positive for recurrence (lymph node metastasis, local recurrence and metastasis to the lung or bone in three, two and two patients, respectively). Clinicopathological parameters for each of the examined patients are summarized in supplementary Table S1, available at *Carcinogenesis* Online. This study was approved by the Ethics Committee of the National Cancer Center, Tokyo, Japan and was performed in accordance with the Declaration of Helsinki 1995. All patients gave their informed consent prior to their inclusion in this study.

Array CGH analysis

High-molecular-weight DNA from fresh-frozen tissue samples was extracted using phenol–chloroform, followed by dialysis. Array CGH was performed using a Human Genome CGH 244K Oligo Microarray Kit (Agilent Technologies, Santa Clara, CA). Labeling and hybridization were performed according to the manufacturer's protocol (Protocol v4.0, June 2006). Briefly, 2 μg of DNA from the patient and from a sex-matched control were double digested with AluI and RsaI (Promega, Madison, WI) for 2 h at 37°C. The digested DNA was then labeled by random priming using an Agilent Genomic DNA Labeling Kit Plus. Patient DNA and control DNA were labeled with Cy5-dUTP and Cy3-dUTP, respectively, and the labeled DNAs were hybridized with human Cot I DNA at 65°C with rotation for 40 h. Arrays were analyzed using the Agilent DNA microarray scanner and the Agilent Feature Extraction software. Presentation of the results was obtained using the Agilent CGH Analytics software package.

The results of array CGH were validated by FISH analysis. An LSI p16 (9p21) SpectrumOrange/CEP 9 SpectrumGreen Probe and an LSI p53 (17p13.1) SpectrumOrange Probe (Abbott/Vysis, Abbott Park, IL), corresponding to the CDKN2A and TP53 loci, respectively, were used. The FISH probes were hybridized to 5 μm thick sections of formalin-fixed, paraffin-embedded tissue specimens taken from a region immediately adjacent to that from which the corresponding fresh-frozen sample had been obtained within the same UC. Nuclei were stained with 4,5-diamidino-2-phenylindole.

BAC array-based methylated CpG island amplification

Because DNA methylation status is known to be organ specific (32), the reference DNA for analysis of the developmental stages of UCs should be obtained from the urothelium and not from other tissues or peripheral blood. Therefore, a mixture of normal urothelial DNA obtained from 11 male patients (C19 to C29) and 6 female patients (C30 to C35) without UCs was used as a reference for analyses of male and female test DNA samples, respectively. Of these 17 patients, 13 and 4 had undergone nephrectomy for renal cell carcinoma and nephrectomy for retroperitoneal sarcoma around the kidney, respectively. The mean age of the patients from whom normal urothelia had been obtained was 66.18 ± 10.49 (mean ± standard deviation) years (range 54–82 years). DNA methylation status was analyzed by BAMCA using a custom-made array (molecular cytogenetics Whole Genome Array-4500) harboring 4361 bacterial artificial chromosome (BAC) clones located throughout chromosomes 1–22, X and Y (33), as described previously (34,35). In 40 samples of UCs (T1 to T40), BAMCA had been performed and the results have already been published (26). For the present study, BAMCA was performed on nine additional samples of UCs (T41 to T49), and correlations between DNA methylation status and copy number alterations were examined in all 49 UCs.

Methylation-specific PCR and combined bisulfite restriction enzyme analysis

DNA methylation status on 5 C-type CpG islands was analyzed by methylation-specific polymerase chain reaction (MSP) and combined bisulfite restriction enzyme analysis (COBRA), as described previously (36). Briefly, bisulfite conversion was carried out using a CpGenome DNA Modification Kit (Chemicon International, Temecula, CA). DNA methylation status on CpG islands of the p16 and hMLH1 genes was determined by MSP using the primers described previously (36). The DNA methylation status of the methylated in tumor (MINT)-1, MINT-2 and MINT-12 clones was determined by COBRA using previously described primers and restriction enzymes (36). In 40 samples of UCs (T1 to T40), MSP and COBRA had been performed and the results have already been published (26). For the present study, MSP and COBRA were performed on nine additional samples of UCs (T41 to T49), and correlations between DNA methylation status and copy number alterations were examined in all 49 UCs.

Statistics

Correlations between copy number alterations and clinicopathological parameters of UCs were analyzed using the unpaired *T*-test. Based on Bonferroni correction for multiplicity of testing, differences at $P < 0.00714$ were considered significant. Unsupervised two-dimensional hierarchical clustering analysis of UCs was done using GeneSpring GX 10.0. Differences in the average number of array CGH probes showing copy number alterations, the average number of BAC clones showing DNA methylation alterations (hypo- and hypermethylation) and the average number of C-type CpG islands showing DNA methylation in UCs belonging to clusters A, B_1 and B_2 yielded by the unsupervised hierarchical clustering were analyzed using the Kruskal–Wallis test. Differences at $P < 0.05$ were considered significant.

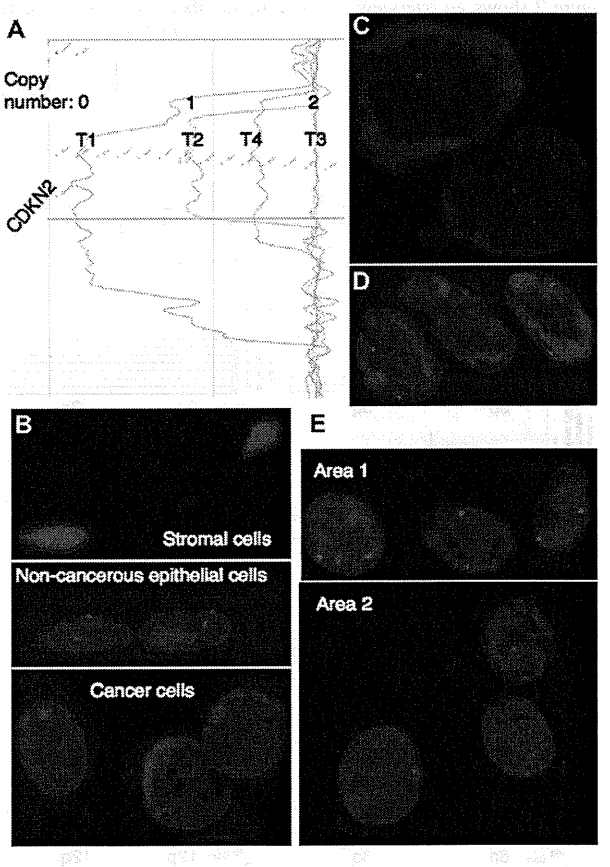

Fig. 1. Validation of array CGH analysis by FISH. (**A**) Array CGH profiles of representative tissue specimens (T1 to T4). The signal ratios of the CDKN2 locus in T1, T2 and T3 corresponded to copy numbers of 0, 1 and 2, respectively, whereas the signal ratio in T4 did not correspond to any whole number. (**B**) Although the LSI p16 (9p21) SpectrumOrange/CEP 9 SpectrumGreen Probe corresponding to the CDKN2A gene revealed two signals in stromal cells and adjacent non-cancerous urothelial cells, it revealed no signal in cancer cells in T1. (**C**) FISH analysis using the same probe revealed one signal in cancer cells in T2. (**D**) FISH analysis using the same probe revealed two signals in cancer cells in T3. (**E**) FISH analysis using the same probe revealed copy number heterogeneity in T4: cancer cells in areas 1 and 2 showed two signals and one signal within a tumor, respectively. These findings can explain the array CGH profile of T4 in panel (A).

Results

Validation of array CGH analysis by FISH

The array CGH analysis for copy number alterations was validated by FISH. Examples of array CGH profiles and FISH images of the four representative UCs (T1 to T4) are shown in Figure 1A–E, respectively. The signal ratios of the CDKN2A locus in T1, T2 and T3 corresponded to copy numbers of 0, 1 and 2, respectively, whereas the signal ratio in T4 did not correspond to any whole numbers (Figure 1A). The LSI p16 (9p21) SpectrumOrange/CEP 9 SpectrumGreen Probe corresponding to the CDKN2A gene revealed two signals in stromal cells and adjacent non-cancerous urothelial cells on the specimen of T1 (Figure 1B). The probe revealed zero, one and two signals in cancer cells in T1, T2 and T3, respectively (Figure 1B–D). FISH analysis revealed copy number heterogeneity within a UC: cancer cells showing two signals and those showing one signal were both observed in T4 (Figure 1E). These findings were able to explain the array CGH profile in T4 (Figure 1A). Similarly FISH analysis using the LSI p53 (17p13.1) SpectrumOrange Probe corresponding to the TP53 gene also validated the array CGH profiles (data not shown).

Copy number alterations and their clinicopathological impact in UCs

Figure 2 shows an overview of the copy number alterations on chromosomes 1–22 in all examined UCs. Chromosomal regions in which the incidence of copy number alterations in all examined UCs were ≥20% are summarized in Table I. If a UC showed copy number heterogeneity like that of T4 in Figure 1, the copy number observed in the major area within the tumor was described as the copy number of the UC in Figure 2 and Table I. On 3q26.1 and 4q13.2 (arrows in Figure 2), the incidence of homozygous deletion (copy number 0) on only 10 and 11 continuous oligonucleotide probes was high (59.2 and 67.3%, respectively, Table I). Although copy number polymorphism has been reported in the above region on 3q26.1, the UGT2B17 gene, which may be associated with smoking-related cancers (37), is the only gene reported to be located within the homozygously deleted region on 4q13.2.

Chromosomal loci on which copy number alterations were significantly correlated with clinicopathological parameters of UCs are shown in Figure 2. The clinicopathological impacts of the copy number alterations are also summarized in Figure 3. For example, loss of 1p32.2–p31.3 was correlated with UC recurrence. Loss of 2q33.3–q37.3 was correlated with higher histological grade. Gain of 3q26.32–q29 was correlated with vascular involvement. Loss of 4p15.2–q13.1 was correlated with higher histological grade. Losses of 5q13.3–q35.3 and 5q14.1–q23.1 were correlated with higher histological grade and tumor configuration (development of non-papillary tumors), respectively. Loss of 6q14.1–q27 was correlated with both lymph vessel involvement and tumor configuration. Gains of 7p21.2–p21.12, 7p11.2–q11.22 and 7p11.2–q11.23 were correlated with deeper invasion, tumor

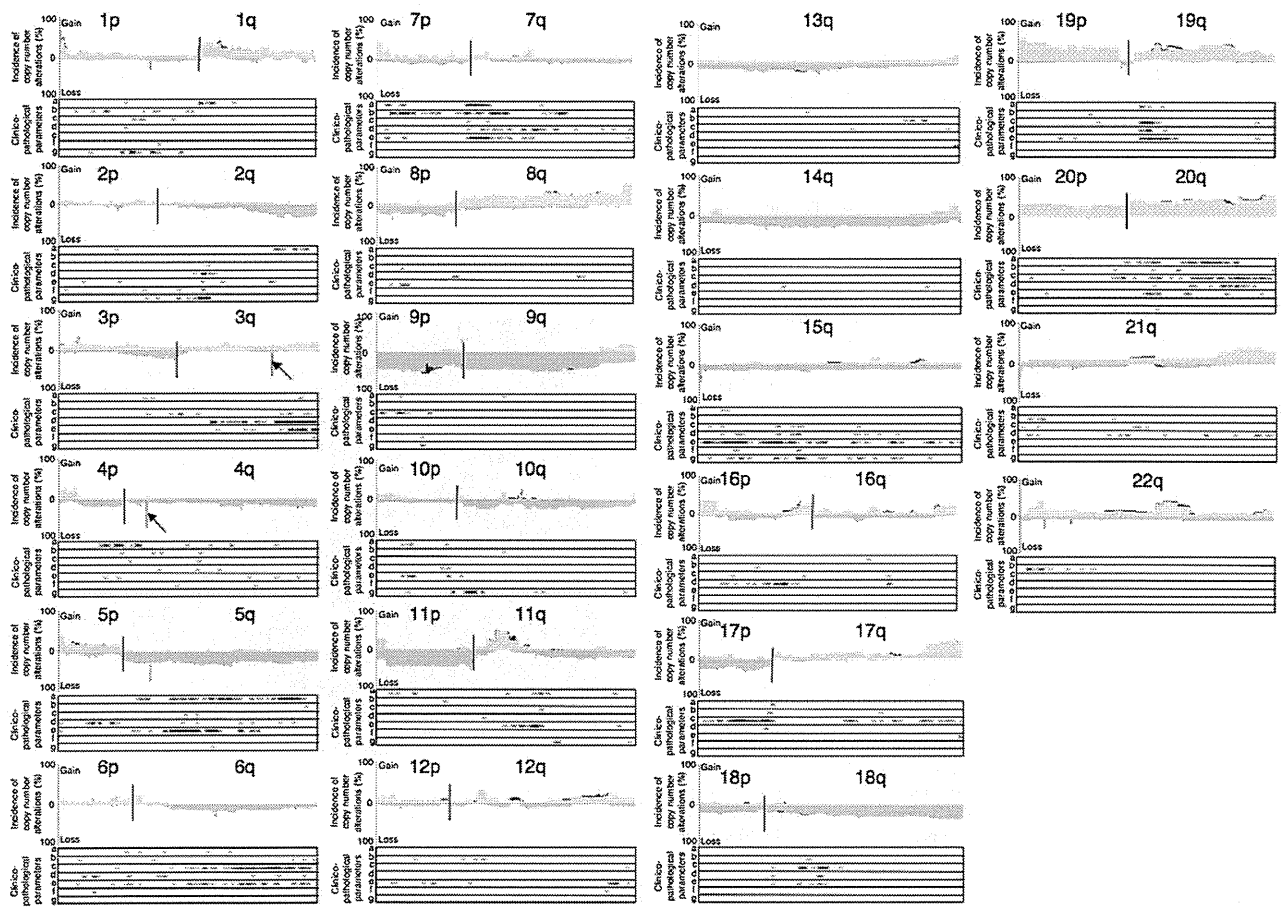

Fig. 2. Copy number alterations and their clinicopathological impacts in UCs. The incidence of copy number alterations on chromosomes 1–22 in UCs (T1 to T49) is shown. Gains (copy number: ≥3) and losses (copy number: 1 or 0) are shown in the upper and lower halves, respectively. Copy numbers of 0, 1, 3 and more are shown in dark red, light red, light blue and dark blue, respectively. The homozygously deleted regions on 3q26.1 and 4q13.2 are indicated by arrows. Locations of the array CGH probe on which copy number alterations were significantly correlated (unpaired *T*-test with Bonferroni correction, $P < 0.00714$) with histological grade (a), depth of invasion (b), lymph vessel involvement (c), vascular involvement (d), tumor configuration (papillary versus non-papillary, (e) lymph node metastasis (f) and recurrence (g) of UCs are indicated by 'X' under each of the histograms for chromosomes 1–22.

Table I. Copy number alterations showing incidences of >20% in the examined UCs

Chromosomal loci	Regions[a]	CN[b]	LI[c]	HI[d]	Chromosomal loci	Regions[a]	CN[b]	LI[c]	HI[d]
1p36.33–1p36.31	000554287–006656854	3	22.4	65.3	10q21.1–10q21.3	057989564–069900014	1	20.4	26.5
1p36.21–1p36.12	016167535–020948798	3	20.4	22.4	10q22.1–10q23.1	071904528–073262876	3	20.4	24.5
1p31.1	072550248–072568068	0	20.4	20.4	10q23.1	083089747–087102060	1	20.4	24.5
1q12–1q31.1	142721264–187457065	3	20.4	40.8	10q23.2–10q24.31	089445919–102120260	1	20.4	26.5
1q31.1–1q44	190299165–247190770	3	20.4	30.6	10q25.1–10q26.13	105709333–124981616	1	20.4	26.5
2q32.1–2q32.2	185846809–190742545	1	20.4	20.4	10q26.3	133783634–135066163	3	20.4	22.4
2q32.3–2q37.3	192350477–242717069	1	20.4	32.7	11p15.5–11p15.4	000182372–003270486	3	28.6	32.7
3p25.3	009517826–011146712	3	22.4	26.5	11q21–11q22.1	096386431–097377420	1	20.4	20.4
3p25.2–3p25.1	012038778–015468042	3	20.4	32.7	11q22.1–11q23.3	097429396–116543936	1	20.4	26.5
3p21.31	048346498–050680352	3	20.4	24.5	11q23.3–11q24.2	124714078–125280002	1	20.4	20.4
3p14.1	065390626–065748270	1	20.4	20.4	11q24.2	124714078–125280002	1	20.4	20.4
3p14.1–3p13	068561452–072819381	1	20.4	24.5	11q24.2–11q25	126760808–132830348	1	20.4	22.4
3p12.3	076229787–076504425	1	20.4	20.4	11q25	133367262–133662626	1	20.4	20.4
3p12.3	077466215–078924208	1	20.4	20.4	12p13.33	001767600–002412124	3	20.4	20.4
3p12.3	079019795–079019854	1	20.4	20.4	12p13.31	006172174–007239121	3	20.4	22.4
3p12.3–3p12.2	081674283–083271792	1	20.4	24.5	12q13.13–12q13.2	050511140–053289666	3	22.4	34.7
3q21.3	128095046–130849578	3	20.4	22.4	12q24.23–12q24.31	119012815–122594513	3	20.4	20.4
3q26.1	163997228–164101835	0	51.0	59.2	13q13.3	036216743–038434639	1	20.4	22.4
3q27.1–3q27.2	184336189–186044074	3	20.4	20.4	13q21.1	053204015–057297991	1	20.4	22.4
3q29	194947608–198141010	3	20.4	20.4	13q34	112711763–114123908	3	20.4	22.4
3q29	198287059–1993214468	3	20.4	20.4	14q11.1–14q11.2	018149473–019665348	1	20.4	40.8
4p16.3–4p16.2	000041413–004080171	3	22.4	30.6	14q12	025347676–028443093	1	20.4	20.4
4p16.2–4p16.1	004863024–009205888	3	20.4	30.6	14q12–14q32.31	028746840–101366386	1	20.4	36.7
4p16.1	009410429–009800836	3	20.4	20.4	14q32.33	103609874–105504791	3	20.4	30.6
4q13.2	069057735–069165872	0	38.8	67.3	15q11.1–15q11.2	018683110–020387386	1	24.5	36.7
4q28.3	135481517–138478960	1	22.4	26.5	15q11.2	018683110–019435559	3	20.4	20.4
4q34.1	172444145–173706467	1	20.4	20.4	15q21.3	054364049–055292702	1	20.4	20.4
4q34.2–4q35.1	176641828–183811059	1	20.4	24.5	15q24.1–15q24.2	072125930–073833248	3	20.4	20.4
4q35.1	184728685–184971082	1	20.4	20.4	16p13.3	000028087–003208434	3	22.4	36.7
4q35.1–4q35.2	186466884–190719413	1	20.4	24.5	16p13.2	007398132–007610763	1	20.4	20.4
5p15.33	000075149–004092634	3	20.4	46.9	16p11.2	028394123–031439837	3	20.4	32.7
5p15.32–5p15.2	005757937–010857368	3	20.4	22.4	16q21	057623929–059070656	1	20.4	20.4
5p15.2–5p15.1	014200030–016428467	3	20.4	20.4	16q22.1	065296755–066623461	3	20.4	22.4
5q11.1–5q35.3	049595677–180644869	1	22.4	63.3	16q24.1–16q24.3	083207007–088690615	3	20.4	26.5
6p21.33–6p21.32	031497746–032281493	3	20.4	24.5	17p13.3–17p11.2	000029169–020234630	1	20.4	32.7
6p21.32–6p21.31	033247001–034187994	3	20.4	20.4	17q11.2	023533773–024473421	3	20.4	20.4
6p21.2–6p21.1	040188750–044391792	3	20.4	24.5	17q21.2–17q21.31	037792629–038922402	3	20.4	20.4
6q16.3–6q21	101107740–105665855	1	20.4	22.4	17q21.31	039360337–041458716	3	20.4	20.4
6q21–6q22.2	113047208–117916793	1	20.4	20.4	17q21.32–17q21.33	043930335–046303881	3	20.4	24.5
7p22.2	000140213–003449208	3	20.4	42.9	17q24.3–17q25.3	067481954–078653589	3	20.4	49.0
7p22.2–7p22.1	003871971–005993219	3	20.4	28.6	18p11.32–18p11.23	000004316–008103527	1	20.4	22.4
7p13	043944978–045169498	3	20.4	24.4	18p11.21	013020518–013601674	1	20.4	20.4
7q11.23	072356188–075985576	3	22.4	22.4	18q11.2	019251951–019903282	1	20.4	20.4
7q22.1	099307676–102120122	3	20.4	30.6	18q12.1–18q23	023887204–076111023	1	20.4	36.7
8p23.2–8p23.1	002209252–006655643	1	20.4	22.4	19p13.3–19p13.11	000064418–019716580	3	28.6	53.1
8p23.1	007040596–008140129	1	24.5	32.7	19q12–19q13.42	032981858–061360576	3	20.4	42.9
8p22	013056908–018810539	1	20.4	22.4	20p13–20q13.33	000008747–062379118	3	26.5	57.1
8p21.3–8p21.2	023372368–027249779	1	20.4	24.5	21p11.2	009896630–013600286	1	20.4	34.7
8p21.1–8p12	027678573–037057454	1	20.4	28.6	21q22.3	041606431–046914745	3	20.4	38.8
8q11.1–8q24.3	047062121–146264902	3	20.4	61.2	22q11.21	016646613–019038934	3	22.4	44.9
9p24.3–9p11.2	000153131–044199460	1	20.4	53.1	22q11.21	018989547–018989606	0	20.4	20.4
9p11.2–9q34.3	045419207–140241935	1	20.4	51.0	22q11.21	019835358–020440240	3	20.4	24.5
9p21.3	021698371–022372349	0	20.4	26.5	22q11.23	021944430–022991816	3	20.4	22.4
9p12–9p11.2	041970428–046018111	3	26.5	36.7	22q12.3–22q13.1	034773534–038422701	3	20.4	40.8
9p24.3	000153131–140241935	1	20.4	53.1	22q13.3–22q13.33	049000786–049565875	3	20.4	20.4
9q34.2–9q34.2	135191259–139424835	3	20.4	22.4					

[a]Based on NCBI36/hg18.
[b]Copy number (If a UC shows copy number heterogeneity, the copy number observed in the major area within the tumor is considered to be the copy number of the UC).
[c]Lowest incidence of copy number alterations in the chromosomal regions (%).
[d]Highest incidence of copy number alterations in the chromosomal regions (%).

configuration and higher histological grade, respectively. Loss of 8p22–p21.3 was correlated with tumor configuration. Loss of 10q11.23–q21.1 was correlated with UC recurrence. Loss of 11q13.5–q14.1 was correlated with tumor configuration. Losses of 15q11.2–q22.2 and 15q21.3 were correlated with tumor configuration and recurrence, respectively. Loss of 16p12.2–p12.1 was correlated with vascular involvement of UCs. Loss of 17p13.3–q11.1 was correlated with lymph vessel involvement. Gain of 19q13.12–q13.2 was correlated with lymph vessel involvement and tumor configuration. Gains of 20q13.12–q13.2 and 20q13.12–q13.33 were correlated with higher histological grade and lymph vessel involvement, respectively. On the other hand, although the incidences of 8q gain and 9p, 11p and 14q loss were generally high in UCs, such copy number alterations were not evidently correlated with any clinicopathological parameters.

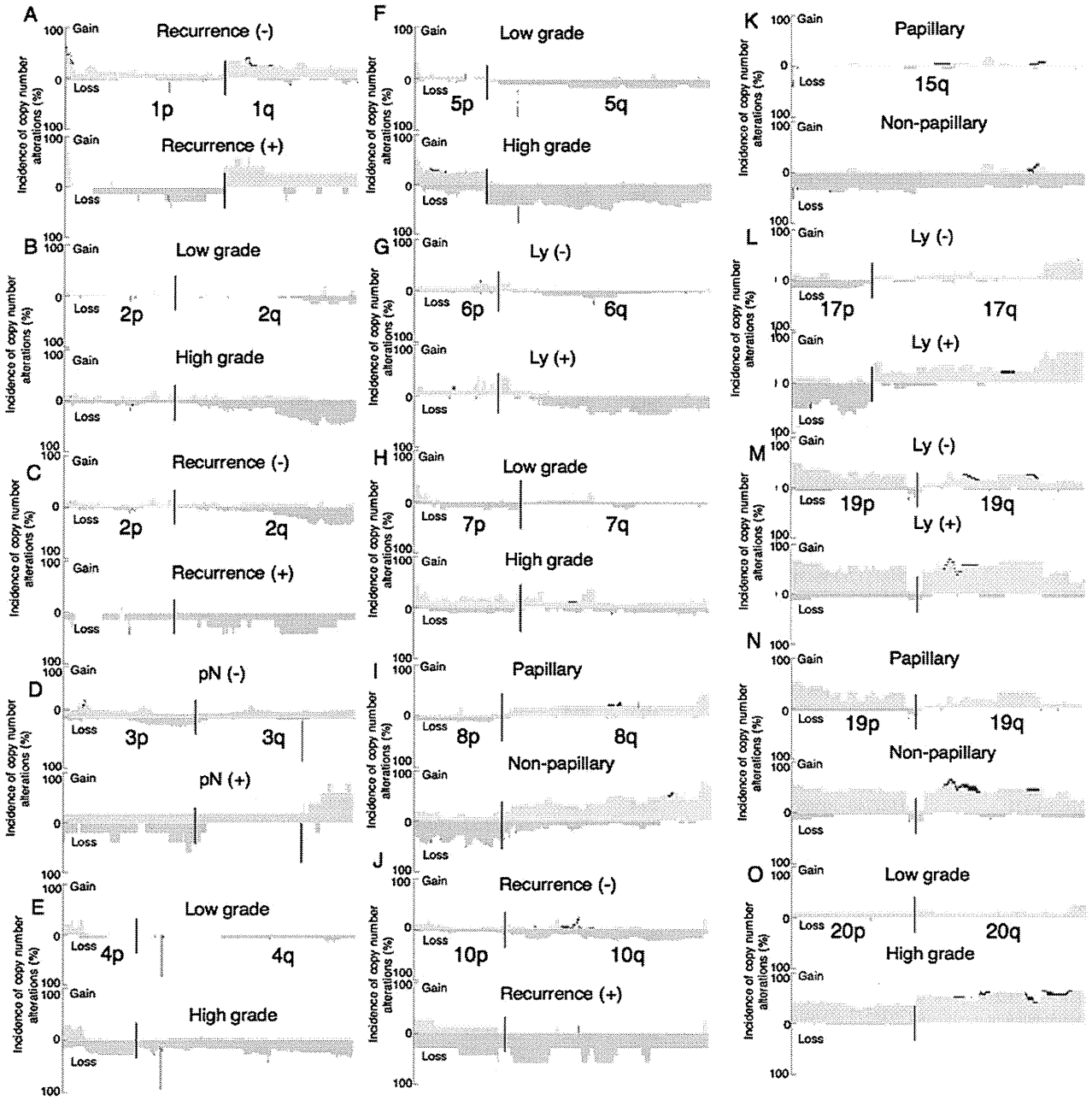

Fig. 3. Correlations between copy number alterations on representative chromosomes and clinicopathological parameters of UCs. The 49 UCs (T1 to T49) were divided into recurrence-negative (n = 42) and -positive (n = 7) cases (**A**, **C** and **J**), histologically low-grade (n = 19) and high-grade (n = 30) tumors (**B**, **E**, **F**, **H** and **O**), lymph node metastasis (pN)-negative (n = 44) and -positive (n = 5) tumors (**D**), lymph vessel involvement (Ly)-negative (n = 33) and -positive (n = 16) tumors (**G**, L and **M**), and papillary (n = 28) and non-papillary (n = 21) tumors (**I**, **K** and **N**). –, negative; +, positive. The incidence of copy number alterations on chromosomes 1 (A), 2 (B and C), 3 (D), 4 (E), 5 (F), 6 (G), 7 (H), 8 (I), 10 (J), 15 (K), 17 (L), 19 (M and N) and 20 (O) in each of the UC groups is shown. Gains (copy number: ≥3) and losses (copy number: 1 or 0) are indicated in the upper and lower halves, respectively. Copy numbers of 0, 1, 3 and more are shown in dark red, light red, light blue and dark blue, respectively.

Unsupervised hierarchical clustering of UCs based on array CGH data

Using two-dimensional unsupervised hierarchical clustering analysis based on copy numbers and all array CGH probes, the 49 UCs were clustered into three subclasses, clusters A, B_1 and B_2 (Figure 4), which contained 4, 12 and 33 tumors, respectively. The average number of probes on which loss (copy number 1 or 0) or gain (≥3) was detected was significantly higher in cluster A (99 499 ± 29 879) than in cluster B_1 (63 324 ± 40 064) and cluster B_2 (46853 ± 35000, P = 0.0271). As shown in Table II, the average number of probes on which gain (≥3) was detected was significantly higher in cluster A than in clusters B_1 and B_2 (P = 0.0153), whereas the difference in the average number of probes on which loss (1 or 0) was detected among clusters A, B_1 and B_2 did not reach statistical significance. The average number of probes on which a copy number of >3 was detected was significantly higher in cluster A than in clusters B_1 and B_2 (P = 0.0053). These data indicated

that copy number alterations, especially chromosomal gain, were accumulated in cluster A in comparison with clusters B_1 and B_2.

Correlation between genetic clustering of UCs and DNA methylation status revealed by BAMCA, MSP and COBRA

As shown in Table II, the average number of BAC clones showing DNA hypomethylation was significantly higher in cluster A than in clusters B_1 and B_2 ($P = 0.0487$), whereas there were no significant differences in the average number of BAC clones showing DNA hypermethylation among the three clusters. The incidence of DNA methylation on CpG islands of the p16 and hMLH1 genes and the MINT-1, MINT-2 and MINT-12 clones was 11 of 49 (detected/analyzed, 22.4%), 1 of 49 (2.0%), 9 of 49 (18.4%), 1 of 49 (2.0%) and 11 of 49 (22.4%), respectively. As shown in Table II, the average number of methylated C-type CpG islands was significantly higher in cluster B_1 than in clusters A and B_2 ($P = 0.0412$). Taken together, the data suggested that copy number alterations associated with overall DNA hypomethylation and regional DNA hypermethylation on C-type CpG islands were accumulated in clusters A and B_1, respectively, when defined on the basis of copy number alterations.

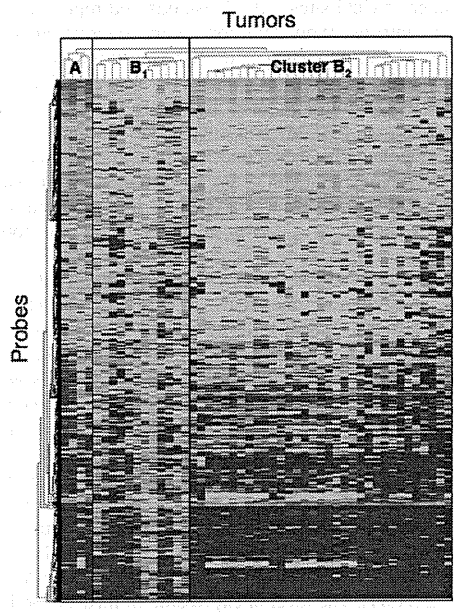

Fig. 4. Unsupervised two-dimensional hierarchical clustering analysis based on array CGH analysis of UCs (T1 to T49). Forty-nine patients with UCs were hierarchically clustered into three subclasses, clusters A ($n = 4$), B_1 ($n = 12$) and B_2 ($n = 33$), based on copy numbers. Copy numbers of 0 or 1 (loss), 2 (no change) and ≥3 (gain) on each probe are shown in blue, yellow and red, respectively. The cluster trees for tumors and probes are shown at the top and to the left of the panel, respectively.

Discussion

We and other groups have demonstrated copy number alterations in UCs for each chromosome or chromosome arm by Southern blotting, PCR–LOH and CGH analyses (3,4,6,7,9–11,25). Several array CGH analyses of UCs have also been performed using tiling BAC arrays (15,16,18). However, such analyses were unable to define the break points in detail. We here examined copy number alterations in UCs using a high-resolution (244K) oligonucleotide array capable of defining break points more precisely.

Copy numbers not corresponding to whole numbers were detected in the array CGH profiles of some UCs. In such cases, FISH analysis revealed copy number heterogeneity even within a single UC (e.g. cancer cells showing both two signals and one signal can be seen in T4 in Figure 1E). In UCs, heterogeneity of cellular atypia is frequently observed in histological specimens: a small area showing higher grade cellular atypia develops within a low-grade UC or cancer cells gain higher grade cellular atypia before they start to disrupt the basal membrane and invade into subepithelial tissues. It is feasible that copy number heterogeneity corresponds to such histological heterogeneity during the multistep malignant progression of UCs.

Our meticulous examination revealed the clinicopathological impacts of copy number alterations at various chromosomal loci (Figures 2 and 3). Losses (copy number 1 or 0) of 2q33.3–q37.3, 4p15.2–q13.1 and 5q13.3–q35.3 and gains (copy number ≥3) of 7p11.2–q11.23 and 20q13.12–q13.2 were significantly correlated with higher histological grade of UCs. Gain of 7p21.2–p21.12 was significantly correlated with deeper invasion. Losses of 6q14.1–q27 and 17p13.3–q11.1 and gains of 19q13.12–q13.2 and 20q13.12–q13.33 were significantly correlated with lymph vessel involvement. Loss of 16p12.2–p12.1 and gain of 3q26.32–q29 were significantly correlated with vascular involvement. Losses of 5q14.1–q23.1, 6q14.1–q27, 8p22–p21.3, 11q13.5–q14.1 and 15q11.2–q22.2 and gains of 7p11.2–q11.22 and 19q13.12–q13.2 were significantly correlated with tumor configuration (development of a non-papillary

Table II. Correlation between genetic clustering of UCs and copy number alterations and DNA methylation status

Copy number and DNA methylation status	Genetic clustering of UCs		
	Cluster A	Cluster B_1	Cluster B_2
Average numbers of array CGH probes showing copy number alterations			
Loss (1 or 0)	24 525 ± 15404	40 826 ± 31644	26 448± 28 462
Gain (≥3)	74 974± 38013*	22 498 ± 15484	20 405 ± 17 369
Gain (>3)	1897 ± 1001†	236 ± 315	209 ± 361
Average numbers of BAC clones showing DNA methylation alterations			
DNA hypomethylation	312 ± 44‡	189 ± 95	236± 91
DNA hypermethylation	334± 85	254± 112	287± 77
Average numbers of C-type CpG islands showing DNA methylation	0.75 ± 0.96	1.33 ± 0.98§	0.58 ± 0.79

*$P = 0.0153$ to clusters B_1 and B_2.
†$P = 0.0053$ to clusters B_1 and B_2.
‡$P = 0.0487$ to clusters B_1 and B_2.
§$P = 0.0412$ to clusters A and B_2.

tumor). Possibly affected genes, which are located at such chromosomal loci and for which correlations with growth, motility and invasiveness of tumor cells and tumorigenesis have already been reported, are listed in supplementary Table S2, available at *Carcinogenesis* Online. Significant correlations between copy number alterations on such loci and clinicopathological parameters reflecting the malignant potential of UCs may be at least partly attributable to silencing or activation of the listed genes. Moreover, such chromosomal loci are important targets for exploration of unidentified tumor-related genes that participate in the malignant progression of UCs; the products of such genes may become target molecules for therapy of UCs. In addition, losses of 1p32.2–p31.3, 10q11.23–q21.1 and 15q21.3 were significantly correlated with recurrence of UCs: copy numbers at such chromosomal loci may become indicators for prognostication of patients with UCs (estimation of recurrence risk using surgically resected specimens).

On the other hand, although the incidence of gain of the entire arm of chromosome 8q and losses of the entire arm of chromosomes 9q, 11p and 14q were not significantly correlated with any of the examined clinicopathological parameters reflecting the malignant potential of UCs, the incidence of such copy number alterations was generally high. Such copy number alterations may occur in the earlier stage of development of both papillary and non-papillary UCs. Therefore, gatekeeper genes for urothelial carcinogenesis may exist on 8q, 9q, 11p and 14q. Combinations of the copy numbers of 8q, 9q, 11p and 14q could become applicable as indicators for the early diagnosis of UCs based on examination of urinary sediments and tissue specimens.

Moreover, the incidence of homozygous deletion on only 11 continuous oligonucleotide probes on 4q13.2 was high (67.3%) and the UGT2B17 gene is located within this homozygously deleted lesion. Copy number polymorphism of the UGT2B17 gene is reportedly associated with smoking-related cancer development (37), and a significant association between UCs and smoking has been demonstrated epidemiologically (38). Since there are many family genes, the exact copy numbers of the UGT2B17 gene were evaluated by quantitative PCR using specific primer sets (supplementary Table S3 is available at *Carcinogenesis* Online). Levels of expression of messenger RNA (mRNA) for the UGT2B17 gene normalized relative to the expression of glyceraldehyde-3-phosphate dehydrogenase mRNA were also examined by quantitative reverse transcription (RT)–PCR analysis (supplementary Table S3 is available at *Carcinogenesis* Online) in 37 of the 49 UCs for which RNA samples were available. Quantitative RT–PCR data for the UGT2B17 gene in 28 UCs showing homozygous deletion (copy number 0) was 3.53 ± 6.40, being significantly lower than that in 9 UCs not showing it (61.61 ± 98.32, $P = 0.008176$). Since the homozygous deletion actually resulted in gene silencing, the correlation between the copy number of the UGT2B17 gene and susceptibility to UCs should be further examined.

UCs were grouped into three subclasses, clusters A, B_1 and B_2, based on copy number alterations. In cluster A, copy number alterations, especially chromosomal gains, revealed by array CGH analysis, and DNA hypomethylation revealed by BAMCA were both accumulated in a genome-wide manner. DNA hypomethylation may result in chromosomal instability through changes in chromatin configuration and enhancement of chromosomal recombination (39). Although such correlation between DNA hypomethylation and chromosomal instability has been observed in experimental models (40) and human immunodeficiency, centromeric instability and facial anomalies syndrome (41) and cancers (25,42), details of the DNA methylation status around each of the chromosome breakpoints are still unclear. UCs in cluster A may be ideal for examination of DNA methylation status around breakpoints to further clarify the molecular mechanisms responsible for chromosomal instability resulting from DNA methylation alterations. Cluster B_1 showed accumulation of regional DNA hypermethylation on C-type CpG islands. In addition, chromosomal losses tended to be accumulated in cluster B_1 in comparison with clusters A and B_2, although such differences did not reach statistical significance. The cancer phenotype associated with accumulation of DNA methylation on C-type CpG islands is defined as the CpG island methylator phenotype, and such accumulation is generally associated with frequent silencing of tumor-related genes due to DNA hypermethylation only and/or a two-hit mechanism involving DNA hypermethylation and LOH in human cancers of various organs (22). Silencing of tumor-related genes due to DNA hypermethylation and chromosomal losses may be critical for the development of UCs belonging to cluster B_1. In cluster B_2, the number of BAC clones showing both DNA hypo- and hypermethylation by BAMCA was rather high, and the number of probes showing loss or gain by array CGH was rather low, in comparison with cluster B_1, although such differences did not reach statistical significance. In addition to copy number alterations, genome-wide DNA methylation alterations may also participate in the development of UCs belonging to cluster B_2.

The number of CpG sites in CpG islands and repetitive sequences in 5′ regions, introns, exons and non-coding regions on BAC clones showing DNA hypomethylation in UCs are summarized in supplementary Table S4, available at *Carcinogenesis*. DNA hypomethylation was observed in BAC clones including both CpG islands and repetitive sequences, possibly resulting in activation of tumor-related genes and/or parasitic elements and loss of chromosomal integrity.

Silencing of representative genes on affected chromosomal loci was confirmed using quantitative RT–PCR analysis (supplementary Table S3 is available at *Carcinogenesis* Online). Although DNA methylation of the p16 gene was detected using MSP, quantitative examination using pyrosequencing (supplementary Table S3 is available at *Carcinogenesis* Online) revealed generally low DNA methylation levels (1.82 ± 0.65%) in all UCs. Therefore, correlations between copy numbers based on array CGH analysis and mRNA expression levels based on quantitative RT–PCR analysis were examined. The p16 gene was silenced in 11 UCs showing homozygous deletion (copy number, 0; quantitative RT–PCR data, 1.24 ± 1.20), whereas the mRNA expression level in 27 UCs not showing it was 104.1 ± 205.11 ($P = 0.00000357$). On the other hand, the DNA methylation level of the CXCL12 gene was 12.59 ± 18.43% for the UCs as a whole. The CXCL12 gene was silenced in 2 UCs with DNA methylation levels of ≥50% (mRNA expression level: 1.81 ± 1.00) but not in 34 UCs with DNA methylation levels of <50% (mRNA expression level: 24.45 ± 34.04). The level of expression of mRNA for the ERBB4 gene in 18 UCs showing a DNA methylation level of ≥5% and/or chromosomal loss (copy number 0 or 1) was 59.1 ± 101.2 and tended to be lower than that in 20 UCs with a DNA methylation level of <5% and a copy number of 2 (128.4 ± 259.3), suggesting the possibility of inactivation due to a combination of DNA hypermethylation and chromosomal loss, although such differences did not reach statistically significant levels. Taken together, the data suggest that genetic and epigenetic alterations (copy number alterations and DNA methylation alterations) are not mutually exclusive during urothelial carcinogenesis. Reflecting the clinicopathological diversity and histological heterogeneity of UCs, genetic and epigenetic events appear to accumulate in a complex manner during the developmental stage of individual tumors.

Supplementary material

Supplementary Tables S1–S4 can be found at http://carcin.oxfordjournals.org/

Funding

Grant-in-Aid for the Third Term Comprehensive 10 Years Strategy for Cancer Control (H19-3-002) from the Ministry of Health, Labor and Welfare of Japan; Grant-in-Aid for Cancer Research (21-2-2) from the Ministry of Health, Labor and Welfare of Japan; Grant (P06012) from the New Energy and Industrial Technology Development Organization (NEDO); Program for Promotion of Fundamental Studies in Health Sciences (10–42) of the National Institute of Biomedical Innovation (NiBio).

Acknowledgements

N.N. is an awardee of a research resident fellowship from the Foundation for Promotion of Cancer Research in Japan.

Conflicts of Interest Statement: None declared.

References

1. Kakizoe,T. *et al.* (1988) Relationship between papillary and nodular transitional cell carcinoma in the human urinary bladder. *Cancer Res.*, **48**, 2299–2303.
2. Kakizoe,T. (2006) Development and progression of urothelial carcinoma. *Cancer Sci.*, **97**, 821–828.
3. Knowles,M. *et al.* (1994) Allelotype of human bladder cancer. *Cancer Res.*, **54**, 531–538.
4. Orlow,I. *et al.* (1995) Deletion of the p16 and p15 genes in human bladder tumors. *J. Natl Cancer Inst.*, **87**, 1524–1529.
5. Sauter,G. *et al.* (1995) c-myc copy number gains in bladder cancer detected by fluorescence *in situ* hybridization. *Am. J. Pathol.*, **146**, 1131–1139.
6. Simoneau,A.R. *et al.* (1996) Evidence for two tumor suppressor loci associated with proximal chromosome 9p to q and distal chromosome 9q in bladder cancer and the initial screening for GAS1 and PTC mutations. *Cancer Res.*, **56**, 5039–5043.
7. Richter,J. *et al.* (1997) Marked genetic differences between stage pTa and stage pT1 papillary bladder cancer detected by comparative genomic hybridization. *Cancer Res.*, **57**, 2860–2864.
8. Wagner,U. *et al.* (1997) Chromosome 8p deletions are associated with invasive tumor growth in urinary bladder cancer. *Am. J. Pathol.*, **151**, 753–759.
9. Hovey,R.M. *et al.* (1998) Genetic alterations in primary bladder cancers and their metastases. *Cancer Res.*, **58**, 3555–3560.
10. Richter,J. *et al.* (1998) Patterns of chromosomal imbalances in advanced urinary bladder cancer detected by comparative genomic hybridization. *Am. J. Pathol.*, **153**, 1615–1621.
11. Simon,R. *et al.* (1998) Chromosomal aberrations associated with invasion in papillary superficial bladder cancer. *J. Pathol.*, **185**, 345–351.
12. Olesen,S.H. *et al.* (2001) Mitotic checkpoint genes hBUB1, hBUB1B, hBUB3 and TTK in human bladder cancer, screening for mutations and loss of heterozygosity. *Carcinogenesis*, **22**, 813–815.
13. Hoque,M.O. *et al.* (2003) Genome-wide genetic characterization of bladder cancer: a comparison of high-density single-nucleotide polymorphism arrays and PCR-based microsatellite analysis. *Cancer Res.*, **63**, 2216–2222.
14. Veltman,J.A. *et al.* (2003) Array-based comparative genomic hybridization for genome-wide screening of DNA copy number in bladder tumors. *Cancer Res.*, **63**, 2872–2880.
15. Blaveri,E. *et al.* (2005) Bladder cancer stage and outcome by array-based comparative genomic hybridization. *Clin. Cancer Res.*, **11**, 7012–7022.
16. Heidenblad,M. *et al.* (2008) Tiling resolution array CGH and high density expression profiling of urothelial carcinomas delineate genomic amplicons and candidate target genes specific for advanced tumors. *BMC Med. Genomics.*, **1**, 3.
17. Zieger,K. *et al.* (2009) Chromosomal imbalance in the progression of high-risk non-muscle invasive bladder cancer. *BMC Cancer*, **9**, 149.
18. Lindgren,D. *et al.* (2010) Combined gene expression and genomic profiling define two intrinsic molecular subtypes of urothelial carcinoma and gene signatures for molecular grading and outcome. *Cancer Res.*, **70**, 3463–3472.
19. Kanai,Y. *et al.* (2007) Alterations of DNA methylation associated with abnormalities of DNA methyltransferases in human cancers during transition from a precancerous to a malignant state. *Carcinogenesis*, **28**, 2434–2442.
20. Kanai,Y. (2008) Alterations of DNA methylation and clinicopathological diversity of human cancers. *Pathol. Int.*, **58**, 544–558.
21. Kanai,Y. (2010) Genome-wide DNA methylation profiles in precancerous conditions and cancers. *Cancer Sci.*, **101**, 36–45.
22. Toyota,M. *et al.* (1999) CpG island methylator phenotype in colorectal cancer. *Proc. Natl Acad. Sci. USA.*, **96**, 8681–8686.
23. Nakagawa,T. *et al.* (2003) Increased DNA methyltransferase 1 protein expression in human transitional cell carcinoma of the bladder. *J. Urol.*, **170**, 2463–2466.
24. Nakagawa,T. *et al.* (2005) DNA hypermethylation on multiple CpG islands associated with increased DNA methyltransferase DNMT1 protein expression during multistage urothelial carcinogenesis. *J. Urol.*, **173**, 1767–1771.
25. Nakagawa,T. *et al.* (2005) DNA hypomethylation on pericentromeric satellite regions significantly correlates with loss of heterozygosity on chromosome 9 in urothelial carcinomas. *J. Urol.*, **173**, 243–246.
26. Nishiyama,N. *et al.* (2010) Genome-wide DNA methylation profiles in urothelial carcinomas and urothelia at the precancerous stage. *Cancer Sci.*, **101**, 231–240.
27. Misawa,A. *et al.* (2005) Methylation-associated silencing of the nuclear receptor 1I2 gene in advanced-type neuroblastomas, identified by bacterial artificial chromosome array-based methylated CpG island amplification. *Cancer Res.*, **65**, 10233–10242.
28. Tanaka,K. *et al.* (2007) Frequent methylation-associated silencing of a candidate tumor-suppressor, CRABP1, in esophageal squamous-cell carcinoma. *Oncogene*, **26**, 6456–6468.
29. Sugino,Y. *et al.* (2007) Epigenetic silencing of prostaglandin E receptor 2 (PTGER2) is associated with progression of neuroblastomas. *Oncogene*, **26**, 7401–7413.
30. Arai,E. *et al.* (2010) DNA methylation profiles in precancerous tissue and cancers: carcinogenetic risk estimation and prognostication based on DNA methylation status. *Epigenomics*, **2**, 467–481.
31. Eble,J.N. *et al.* (2004) Tumours of the Urinary System and Male Genital Organs. World Health Organization Classification of Tumours. Pathology and Genetics. IARC Press, Lyon.
32. Illingworth,R. *et al.* (2008) A novel CpG island set identifies tissue-specific methylation at developmental gene loci. *PLoS Biol.*, **6**, e22.
33. Inazawa,J. *et al.* (2004) Comparative genomic hybridization (CGH)-arrays pave the way for identification of novel cancer-related genes. *Cancer Sci.*, **95**, 559–563.
34. Arai,E. *et al.* (2009) Genome-wide DNA methylation profiles in both precancerous conditions and clear cell renal cell carcinomas are correlated with malignant potential and patient outcome. *Carcinogenesis*, **30**, 214–221.
35. Arai,E. *et al.* (2009) Genome-wide DNA methylation profiles in liver tissue at the precancerous stage and in hepatocellular carcinoma. *Int. J. Cancer.*, **125**, 2854–2862.
36. Arai,E. *et al.* (2006) Regional DNA hypermethylation and DNA methyltransferase (DNMT) 1 protein overexpression in both renal tumors and corresponding nontumorous renal tissues. *Int. J. Cancer.*, **119**, 288–296.
37. Lazarus,P. *et al.* (2005) Genotype-phenotype correlation between the polymorphic UGT2B17 gene deletion and NNAL glucuronidation activities in human liver microsomes. *Pharmacogenet. Genomics.*, **15**, 769–778.
38. Alberg,A.J. *et al.* (2009) Cigarette smoking and bladder cancer: a new twist in an old saga? *J. Natl Cancer Inst.*, **101**, 1525–1526.
39. Jones,P.A. *et al.* (2007) The epigenomics of cancer. *Cell*, **128**, 683–692.
40. Howard,G. *et al.* (2008) Activation and transposition of endogenous retroviral elements in hypomethylation induced tumors in mice. *Oncogene*, **27**, 404–408.
41. Hansen,R.S. *et al.* (1999) The DNMT3B DNA methyltransferase gene is mutated in the ICF immunodeficiency syndrome. *Proc. Natl Acad. Sci. USA*, **96**, 14412–14417.
42. Saito,Y. *et al.* (2002) Overexpression of a splice variant of DNA methyltransferase 3b, DNMT3b4, associated with DNA hypomethylation on pericentromeric satellite regions during human hepatocarcinogenesis. *Proc. Natl Acad. Sci. USA*, **99**, 10060–10065.

Received August 11, 2010; revised December 1, 2010; accepted December 11, 2010

Histopathology

Histopathology 2012, **60**, E12–E18. DOI: 10.1111/j.1365-2559.2012.04174.x

DNA methyltransferase 3B expression is associated with poor outcome of stage I testicular seminoma

Eri Arai,[1] Tohru Nakagawa,[2] Saori Wakai-Ushijima,[1] Hiroyuki Fujimoto[2] & Yae Kanai[1]

[1]*Division of Molecular Pathology, National Cancer Center Research Institute, and* [2]*Department of Urology, National Cancer Center Hospital, Tokyo, Japan*

Date of submission 12 April 2011
Accepted for publication 14 July 2011

Arai E, Nakagawa T, Wakai-Ushijima S, Fujimoto H & Kanai Y
(2012) *Histopathology* **60**, E12–E18

DNA methyltransferase 3B expression is associated with poor outcome of stage I testicular seminoma

Aims: To examine in testicular seminomas the expression of DNA methyltransferase 3B (DNMT3B), which is known to be associated with early embryonic development and carcinogenesis, and to obtain a predictive marker for relapse of stage I seminomas.
Methods and results: Immunohistochemical examination of DNMT3B was performed in 88 cases of seminoma, 35 (39.8%) of which showed widely scattered nuclear immunoreactivity for DNMT3B, and 53 (60.2%) of which were completely negative. The incidence of focal DNMT3B expression was higher in stage III seminomas (5/5, 100%) than in stage I (25/70, 35.7%) or stage II (5/13, 38.5%) seminomas ($P = 0.011$). In stage I seminomas there were no significant correlations between DNMT3B expression and tumour size, invasion of the rete testis, or lymphatic or vascular involvement. Six of 25 cases (24%) showing DNMT3B expression relapsed, whereas only 3/45 cases (6.7%) lacking such expression did so ($P = 0.037$). Patients with seminomas showing DNMT3B expression had a significantly lower relapse-free survival rate than patients whose tumours lacked this feature ($P = 0.0464$).
Conclusions: Patients with seminomas showing focal DNMT3B expression are at increased risk of relapse, and should be followed up carefully.

Keywords: DNA methyltransferase 3B, prognostication, seminoma, testicular germ cell tumour, tumour relapse

Abbreviations: DNMT, DNA methyltransferase; TGCT, testicular germ cell tumour

Introduction

Seminoma is the most common histological subtype of testicular germ cell tumour (TGCT). At initial presentation, approximately 70–80% of patients with seminoma are diagnosed at clinical TNM stage I, i.e. showing no evidence of metastasis. However, 15–20% of them relapse after orchiectomy. As such relapse may occur 5 years or more after orchiectomy,[1] careful long-term follow-up is necessary. However, prolonged follow-up and frequent radiological examinations are burdensome and costly.

Although postoperative radiotherapy of the para-aortic area was the standard choice for several decades,[2] long-term follow-up studies have demonstrated an association of radiotherapy with late complications (i.e. cardiovascular disease[3] and secondary malignancy).[4,5] In recent years, although single-course chemotherapy has yielded survival data equivalent to those after radiotherapy,[6] its associated complications have not yet been evaluated in a long-term follow-up study. To avoid unnecessary treatment or over-frequent surveillance, markers predicting relapse risk are needed.

DNA methylation alterations play an important role in human carcinogenesis.[7] With respect to TGCTs, a difference in methylated genes between seminoma and

Address for correspondence: Y Kanai, Division of Molecular Pathology, National Cancer Center Research Institute, 5-1-1 Tsukiji, Chuo-ku, Tokyo 104-0045, Japan.
e-mail: ykanai@ncc.go.jp

non-seminomatous TGCT has been reported.[8,9] In addition, TGCT originates from male germ cells, and has various histological subtypes resembling the differentiation of fertilized germ cells to embryos. DNA methyltransferase 3B (DNMT3B) is a key enzyme for *de-novo* DNA methylation during the dynamic DNA methylation reprogramming that occurs in early embryogenesis.[10] These facts suggest the possible participation of DNMT3B in TGCT development. However, only an association between DNMT3B expression and drug sensitivity of cultured embryonal carcinoma cells[11] has been reported to date, and no studies have examined the clinicopathological significance of DNMT3B expression in TGCT. In this study, we examined the expression of DNMT3B protein in seminomas and explored the possibility of using it for prognostication.

Materials and methods

PATIENTS AND TISSUE SAMPLES

Eighty-eight testicular seminomas obtained from patients who underwent radical orchiectomy at the National Cancer Center Hospital, Tokyo, Japan were analysed. The mean (±standard deviation) age of the patients was 38.8 ± 9.2 years (range 21–66 years). The pathological diagnosis of TGCT was performed by two pathologists (E.A. and Y.K.), on the basis of the World Health Organization classification.[12]

Initial staging was carried out with a combination of chest X-ray and computed tomography scans. In this cohort, none of the patients received any preoperative therapy for the seminoma. None of the patients with stage I seminomas had received any postoperative therapy until relapse was diagnosed, and they had been under surveillance with chest X-ray, computed tomography scans, and determination of serum tumour marker levels (α-fetoprotein and the β-subunit of human chorionic gonadotropin).

This study was approved by the Ethics Committee of the National Cancer Center, Tokyo, Japan.

ANTIBODY

A polyclonal anti-human DNMT3B antibody was raised by immunizing rabbits with polypeptides corresponding to the C-terminal region of DNMT3B, N-ENKTRRRTADDSATS-C. To confirm the specificity of this antibody, NCC-IT cells, originating from human testicular teratoma,[13] were subjected to western blotting analysis (Figure 1). Total cell extracts were separated by sodium dodecylsulphate (SDS) polyacrylamide gel electrophoresis and transferred electrophoretically to polyvinylidene difluoride (PVDF) filters, which were then incubated with the rabbit anti-human DNMT3B antibody (diluted 1:1000) overnight at 4°C, followed by horseradish peroxidase-linked anti-rabbit immunoglobulin (Amersham Biosciences, Buckinghamshire, UK). Finally, an ECL western blotting detection system (Amersham) was used for detection.

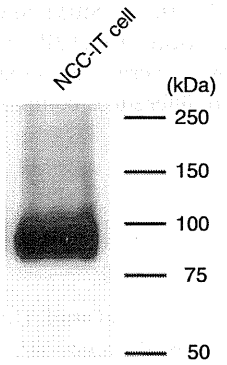

Figure 1. Western blotting with anti-human DNA methyltransferase 3B (DNMT3B) polyclonal antibody. A major immunoreactive band of about 95.8 kDa, corresponding to the molecular mass of DNMT3B, was detected in NCC-IT cells.

IMMUNOHISTOCHEMISTRY

Three-micrometre-thick sections of formalin-fixed, paraffin-embedded tissue specimens of each seminoma were deparaffinized and dehydrated. For antigen retrieval, the sections were heated for 10 min at 120°C in an autoclave. Non-specific reactions were blocked with 2% normal swine serum. All sections were incubated with the rabbit anti-human DNMT3B polyclonal antibody at 4°C overnight, and then with biotinylated secondary antibody (anti-rabbit IgG; dilution 1:200; Vector Laboratories, Burlingame, CA, USA;) at room temperature for 30 min. Following this, the sections were treated with Vectastain Elite ABC reagent (Vector Laboratories), and 3,3′-diaminobenzidine tetrahydrochloride was used as the chromogen. All sections were counterstained with haematoxylin. As a negative control, the primary antibody was omitted from the reaction sequence. Because high-level expression of DNMT3B mRNA has been reported in non-seminomatous TGCT, especially in embryonal carcinoma,[11,14,15] we used three tissue specimens of testicular embryonal carcinoma as positive controls for immunohistochemistry.

STATISTICS

Correlations between focal DNMT3B expression and clinicopathological features were analysed with the

chi-squared test ($P < 0.05$). Survival curves of patients with and without focal DNMT3B expression in their testicular seminomas were calculated by the Kaplan–Meier method, and differences compared using the log-rank test.

Results

DNMT3B EXPRESSION IN TGCT

All three samples of embryonal carcinoma used as positive controls showed diffuse and strong immunoreactivity for DNMT3B (Figure 2A,B). Immunoreactivity was observed in the nuclei, but not in either the cytoplasm or the cell membrane.

In contrast to embryonal carcinomas, most seminomas were completely immunonegative for DNMT3B (Figures 2C,D). However, in some seminomas, tumour cells showing strong nuclear immunoreactivity were scattered among a large majority of tumour cells lacking nuclear immunoreactivity (Figure 2E,F,G).

On the basis of these findings, we considered a seminoma to be positive for (focal) DNMT3B expression when one or more tumour cells per 50 high-power fields showed strong nuclear immunoreactivity equivalent to that of embryonal carcinoma. With the use of this criterion, 35/88 seminomas (39.8%) were considered to be positive. No seminomas showed diffuse immunoreactivity for DNMT3B.

There were no significant morphological differences between the scattered tumour cells showing immunoreactivity and the surrounding tumour cells lacking immunoreactivity in each individual seminoma (Figure 2E,F). Furthermore, there were no significant histological differences between seminomas with focal DNMT3B expression and those lacking it.

CORRELATION BETWEEN FOCAL DNMT3B EXPRESSION AND CLINICOPATHOLOGICAL PARAMETERS OF PATIENTS WITH SEMINOMAS

Table 1 shows the correlation between focal DNMT3B expression and initial tumour stage in patients with seminomas. The incidence of DNMT3B expression was significantly higher in stage III seminomas (100%) than in stage I (35.7%) or stage II (38.5%) seminomas ($P = 0.011$), suggesting that such expression may reflect tumour aggressiveness. Therefore, we analysed the correlation between DNMT3B expression and various clinicopathological parameters in stage I seminomas. There were no significant correlations between expression and tumour size, invasion of the rete testis, invasion of the epididymis, lymphatic or vascular involvement, or invasion of the spermatic cord (Table 2). On the other hand, 9/70 patients with stage I seminoma suffered tumour relapse during follow-up after orchiectomy (metastasis to the retroperitoneal lymph nodes in eight and to the lumbar vertebra and humerus in one). Six of 25 cases (24%) showing DNMT3B expression developed distant metastases, whereas only 3/45 cases (6.7%) lacking expression did so ($P = 0.037$; Table 2).

PROGNOSTIC SIGNIFICANCE OF FOCAL DNMT3B EXPRESSION IN STAGE I SEMINOMA

Figure 3 shows the Kaplan–Meier survival curves of patients with stage I seminomas. The period covered ranged from 15 to 5509 days (mean 1794 days). The relapse-free survival rate of patients with seminomas showing DNMT3B expression was significantly lower than that of patients with seminomas lacking expression ($P = 0.0464$).

Discussion

Postoperative management of stage I seminoma has been the subject of active discussion among clinicians and researchers.[16–18] Although both postoperative radiotherapy and chemotherapy can reduce the rate of relapse in patients with stage I seminomas,[6] patients who do not suffer relapse may be overtreated. As curative chemotherapy is available for metastatic seminoma if it can be detected early, careful surveillance is thought to be an effective strategy for avoiding overtreatment.[17] Estimation of relapse risk may be advantageous for appropriate surveillance planning in individual patients with stage I seminoma.

Several groups have studied prognostic factors in stage I seminoma. On the basis of a pooled analysis, Warde *et al.* reported that tumour size (≤40 mm or >40 mm), invasion of the rete testis and lymphatic or vascular involvement were predictive of relapse on univariate analysis, and that tumour size and invasion of the rete testis remained significant on multivariate analysis.[19,20] However, other papers did not report these factors to be significantly predictive. In our cohort, although lymphatic or vascular involvement was significantly correlated with tumour relapse ($P = 0.0304$), tumour size and invasion of the rete testis were not ($P = 0.1445$ and $P = 0.0566$, respectively, log-rank test). Thus, any prognostic impacts of these clinicopathological parameters are still controversial. Moreover, no significant molecular